NASA Contractor Report 189087

P.67

Cryogenic Magnetic Bearing Test Facility (CMBTF)

AVCON—Advanced Controls Technology, Inc.
Northridge, California

February 1992

Prepared for
Lewis Research Center
Under Contract NAS3–25572

National Aeronautics and Space Administration

TABLE OF CONTENTS

	Page
List of Figures	ii
List of Tables	iii
Forward	iv
1.0 Introduction and Summary	1-1
2.0 Selection of the Type of Magnetic Bearing	2-1
2.1 Literature/Industry Survey	2-1
2.2 Trade Off Study	2-2
3.0 Magnetic Bearing System Analysis	3-1
3.1 Dynamic Analysis	3-1
3.1.1 Rotor Finite Element Dynamic Model	3-1
3.1.2 Output Format	3-3
3.2 Magnetic Analysis	3-4
3.2.1 Requirements Analysis	3-5
3.2.2 Permanent Magnet Circuit Calculations	3-6
3.2.3 Electromagnetic Coil Calculations	3-10
3.2.4 Performance Analysis of Cryogenic Bearing at Room Temperature	3-15
3.3 Ball Bearing Analysis	3-16
3.4 Stress Analysis	3-20
3.5 Thermal Analysis	3-23
3.6 Servo Analysis	3-25
3.6.1 Physical Description	3-25
3.6.2 System Models	3-25
3.6.3 Analysis	3-27
3.7 Lateral Force Generator	3-34
4.0 Magnetic Bearing Radial Actuator Analysis and Design	4-1
5.0 Design, Fabrication, and Assembly of the CMBTF	5-1
6.0 Functional Test of the CMBTF	6-1
7.0 Summary and Conclusions	7-1
8.0 References	8-1

LIST OF ILLUSTRATIONS

Figure		Page
1-1	Cryogenic Magnetic Bearing Test Facility Design	1-4
1-2	Component Parts of CMBTF	1-5
1-3	Permanent Magnet Bias Bearing Stator Assembly	1-5
1-4	CMBTF Prior to Addition of Magnetic Bearing	1-6
1-5	Magnetic Bearing Shaft, Flywheel, Force Generators	1-7
1-6	Load Output Vs. Actuator Input Current	1-8
1-7	Magnetic Bearing System Power Consumption Vs. Load	1-8
3-1	Rotor Finite Element Model	3-1
3-2	Modified Shaft Geometry, Version 8	3-3
3-3	ECDR Drive Belt & Pulley Geometry, Viewed From Above	3-16
3-4	Stiffness Vs. Radial Load	3-17
3-5	Upper Bearing Lube Factor Vs. RPM	3-17
3-6	Forces Acting on the Rotor That Affect Upper Bearing Load	3-19
3-7	Simplified Diagram of System	3-25
3-8	Transfer Function of Filter	3-28
3-9	Bode Plot	3-28
3-10	Actuator Gain and Compensation	3-29
3-11	Computer Model of Actuator	3-29
3-12	Z Channel Analysis	3-30
3-13	Y Channel Analysis	3-31
3-14a	Z Channel Root Locus, Without Notch Filter or Actuator	3-32
3-14b	Z Channel Root Locus, With Notch Filter and Actuator	3-32
3-15	Single Channel Closed Loop Bode Plot	3-33
6-1	Load Output Vs. Actuator Input Current	6-1

LIST OF TABLES

Table		Page
1-1	CMBTF Design Requirements	1-2
1-2	Comparison of Design Approaches	1-3
1-3	Design Criteria and Materials Properties	1-4
2-1	Magnetic Bearing Type Trade-off Study	2-4
3-1	Permanent Magnet Flux Table	3-19
3-2	Bottom Bearing Load and Deflections	3-19
3-3	Bottom Bearing Life and Reliability	3-19
3-4	Summary of Dynamic Stress	3-21
6-1	Results of Performance Tests	6-1
6-2	Magnetic Bearing Actuator Power Consumption	6-2

FOREWORD

This Final Report describes the research and development undertaken to convert a Government owned Eddy Current Damper Rig into a Cryogenic Magnetic Bearing Test Facility (CBMTF) for exploring the potential for applying magnetic bearing technology to Space Shuttle Main Engines (SSME) applications. The start date for the contract was January 18, 1989; and the completed CMBTF was shipped to NASA LeRC on May 29, 1990. The Program was under the direction of Mr. E. DiRusso, NASA Project Manager, NASA LeRC Structural Dynamics Branch, and Mr. C.R. Meeks, AVCON Principal Investigator. Other technical contributors from NASA LeRC included Dr. G. Brown and Mr. A. Kascak. Technical contributors from AVCON included Mr. J. Hulstyn, Mr. K. Nason, Mr. A. Tran, Dr. W. Sunada, Mr. J. Sherman, Mr. V. Spencer, Mr. S. Schwartz, Dr. A. J. Mendez, and Mr. P. Maschack.

1.0 INTRODUCTION and SUMMARY

Recurring problems with Space Shuttle Main Engine bearings have been the impetus for research on new bearing materials/lubricants, and also for magnetic bearing alternatives. New bearing materials/lubricants may be a near term solution, but magnetic bearings are a potential long term solution. Magnetic bearings have historically been too large, heavy, and power consuming. Also, eddy current/hysteresis losses can create shaft heating and structural problems so that improperly designed magnetic bearings would have RPM limitations, excluding them from SSME type applications.

This program had the objective of demonstrating that magnetic bearings could be designed to be significantly smaller, lighter, less power consuming, and without the eddy current/hysteresis heating problems of older technology magnetic bearings. A further objective was to show that these features could be obtained at cryogenic temperatures; the working environment for the SSME.

The objective was met by carrying out a systematic plan to:

- Analyze and design a magnetic bearing for test rig application
- Fabricate a magnetic bearing for incorporation into an existing test rig (Eddy Current Damper Rig).
- Analyze and design the modifications to the Eddy Current Damper Rig to incorporate the magnetic bearing.
- Fabricate new parts, rework existing parts, and reassemble the rig with magnetic bearing parts.
- Test and deliver the modified rig to NASA Lewis Research Center for further tests and evaluation.

The original design requirements for the CMBTF are detailed in Table 1-1.

Parameter	Design Requirement	Test Requirement
Radial Load	2224 N (500 lbs) @ -321° F	2224 N (500 lbs) @ -321° F
Shaft Speed	25,000 RPM (by analysis)	0 - 15,000 RPM
Operating Temperature	Ambient to -321 ° F	Ambient to -321° F
Minimum radial clearance	0.38 mm (0.015 inch)	0.38 mm (0.015 inch)
First critical speed	6,000 to 8,000 RPM	6,000 to 8,000 RPM

Table 1-1. CMBTF Design Requirements

In order to select the optimum magnetic bearing type, a literature/industry survey was conducted. This survey allowed us to identify the state of the art in "enabling technologies" as well as in magnetic bearing system concepts. The data base was used to choose candidate CMBTF designs based on the AVCON Homopolar Permanent Magnet Bias approach (a single pole around the air gap), as well as other design approaches found in the literature/industry survey. State of the art components and materials were also identified for use in our design.

Some of the alternate design approaches were based on analyzing commercially available magnetic bearings. A compendium of the candidate designs is shown in Table 1-2, which depicts the candidates with respect to various operating parameters and physical characteristics. The design criteria and materials properties used for the comparison study are shown in Table 1-3.

It is evident from the comparisons in Table 1-2 that the AVCON HPMB approach is preferable from size, weight, and power aspects. Physical characteristics of the AVCON bearing indicate that it is indeed worth pursuing magnetic bearing technology for SSME applications.

After analytically affirming that the AVCON HPMB approach was best, the project next demonstrated the findings by producing a design to be incorporated into an existing test rig (the ECDR). The modified ECDR, converted into a CMBTF, is shown in Figure 1-1. The various component parts are shown in Figures 1-2 and 1-3. A partial assembly is shown in Figure 1-4.

DESIGN CONCEPT			
	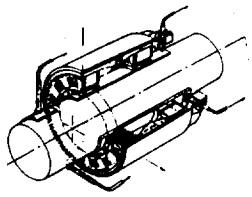	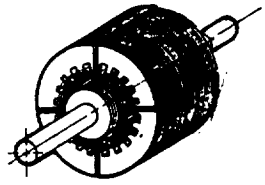	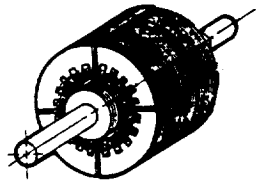
PARAMETER	Permanent Magnet Bias Active Control	All-Electromagnetic (Vanadium Permendure)	Commercial All-Electromagnetic (Catalog Item)
Outside Diameter	5.25 in. (13.3 cm)	7.0 in. (17.8 cm)	10.0 in. (25.4 cm)
Inside Diameter	2.0 in. (5.24 cm)	2.0 in. (5.24 cm)	2.0 in. (5.24 cm)
Length	4.3 in. (8.95 cm)	4.0 in. (10.2 cm)	6.3 in. (16.0 cm)
Max Force Output	500 lb (2224 N)	500 lb (2224 N)	430 lb (1800 N)
Power at Max Force, 70° F	35 Watts	380 Watts	400 Watts
Power at Max Force, -321° F	< 20 Watts	90 Watts	100 Watts
Stead State Power, 70° F	1 Watt	90 Watts	95 Watts
Stead State Power, -321° F	< 1 Watt	< 20 Watts	< 20 Watts
Weight of Actuator	21.4 lbs (9.72 Kg)	43.8 lbs (19.9 Kg)	66 lbs (29.9 Kg)
Remarks:	- Smallest - Lightest Weight - Lowest Power Consumption	Electronics control is larger than PM bias, due to power supply and amplifier for large bias-currents	Electronics control system is over 5 cubic feet in volume

Table 1-2. Comparison of Design Approaches

Parameter	Value
Shaft air gap diameter	7.62 cm (3.0 inches)
Radial stiffness	0.79 x 10^4 N/mm (4.5 x 10^4 lb/in.)
Ferromagnetic material magnetic saturation limit (linear range)	16,000 Gauss
Coil temperature rise	70° C
Permanent magnet energy product	30 x 10^6 Gauss-Oersteds

Table 1-3. Design Criteria and Materials Properties

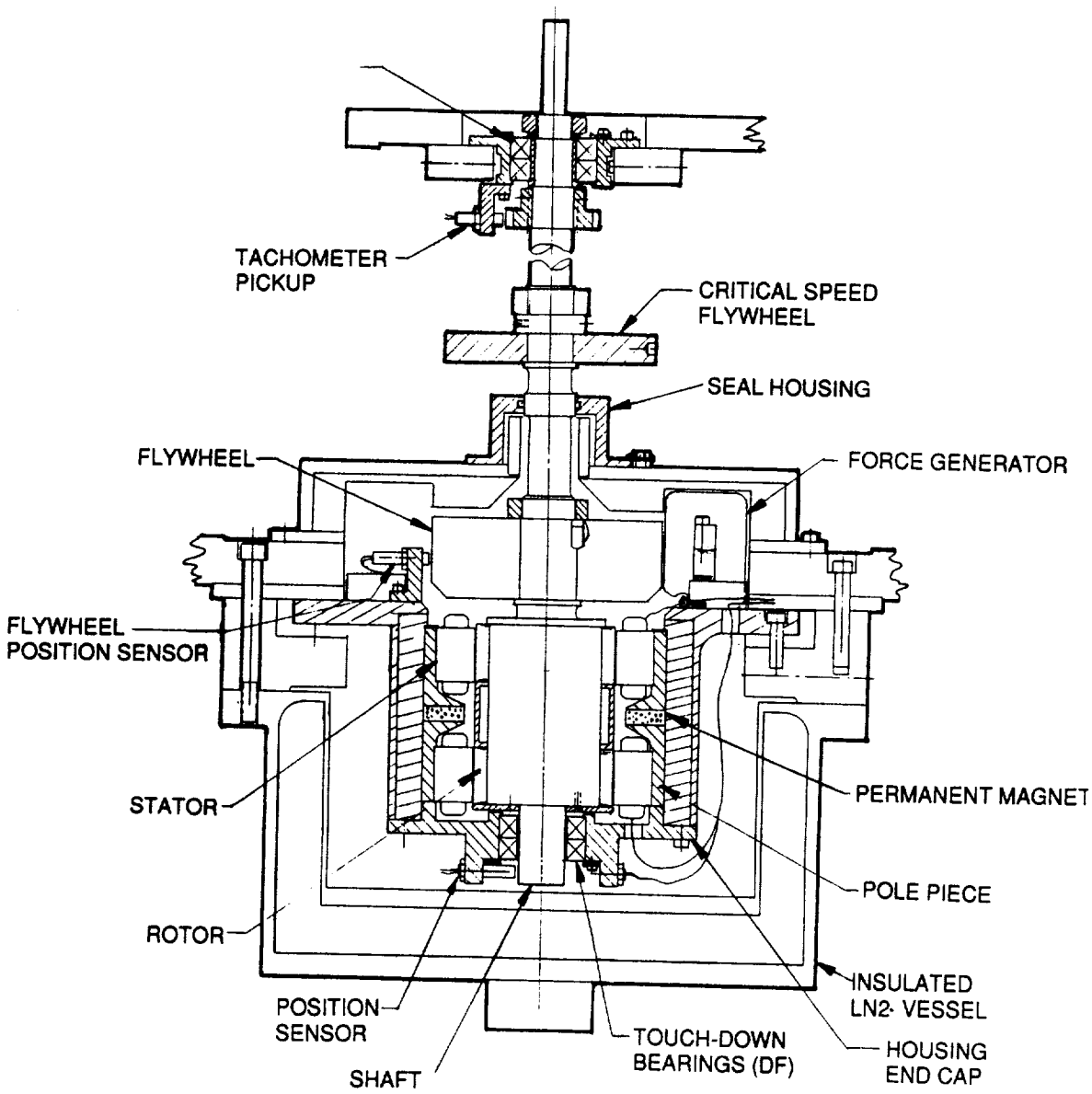

Figure 1-1. Cryogenic Magnetic Bearing Test Facility Design

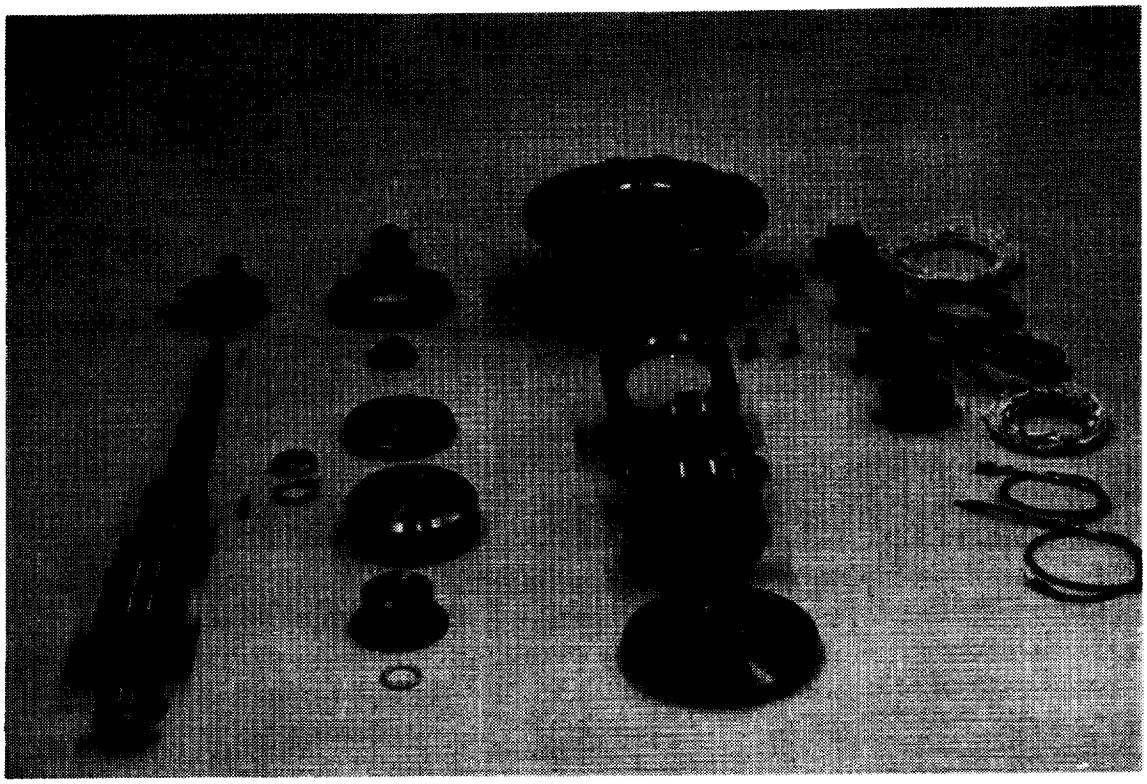

Figure 1-2. Component Parts of CMBTF

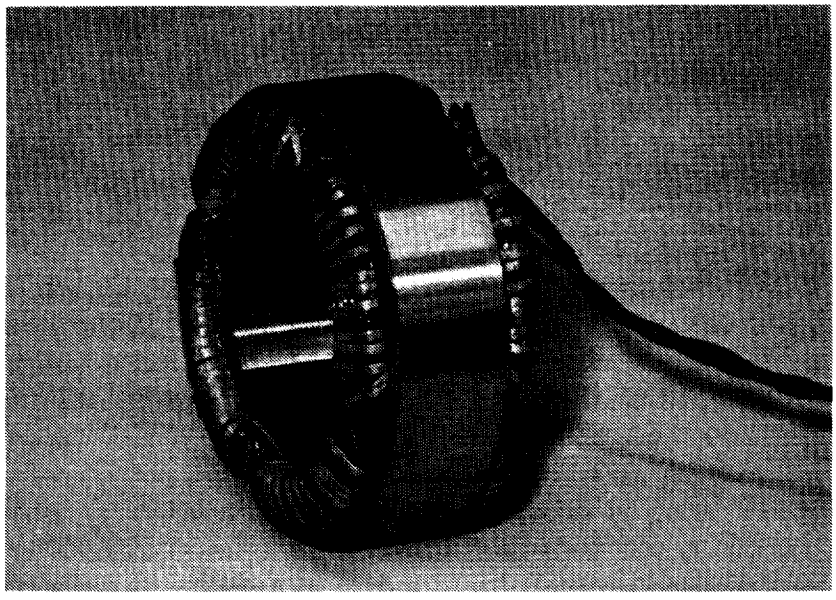

Figure 1-3. Permanent Magnet Bias Bearing Stator Assembly

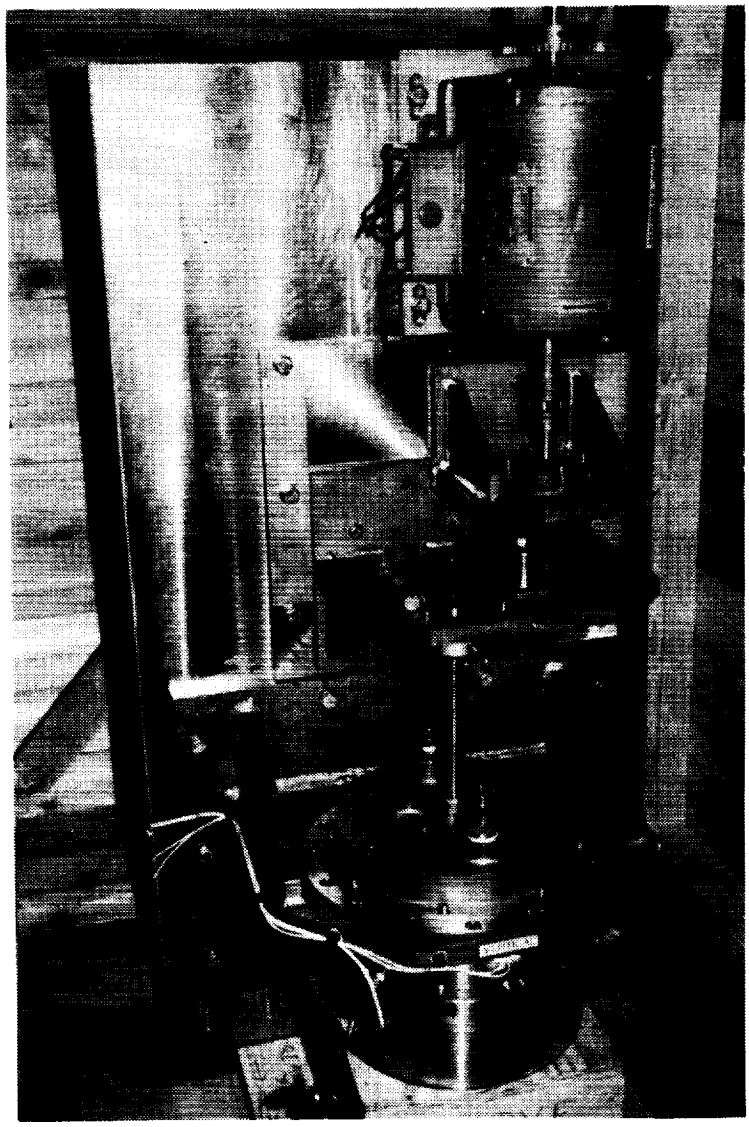

Figure 1-4. CMBTF Prior to Addition of Magnetic Bearing

The CMBTF includes lateral force generators (see Figure 1-5) which permit testing and evaluation under various operating conditions. Testing was done at room temperature with respect to load capacity, radial stiffness, power consumption, speed (RPM), and temperature rise of the coils. Results of these tests are summarized in Section 6.0.

The CMBTF was, by design, optimized both for ambient and cryogenic temperatures by taking the material temperature-dependent characteristics into account. This permits complete testing and evaluation in both temperature regimes. The force (load output) versus actuator current is shown in Figure 1-6. The power dissipation (system and actuator portions) versus load are shown in Figure 1-7.

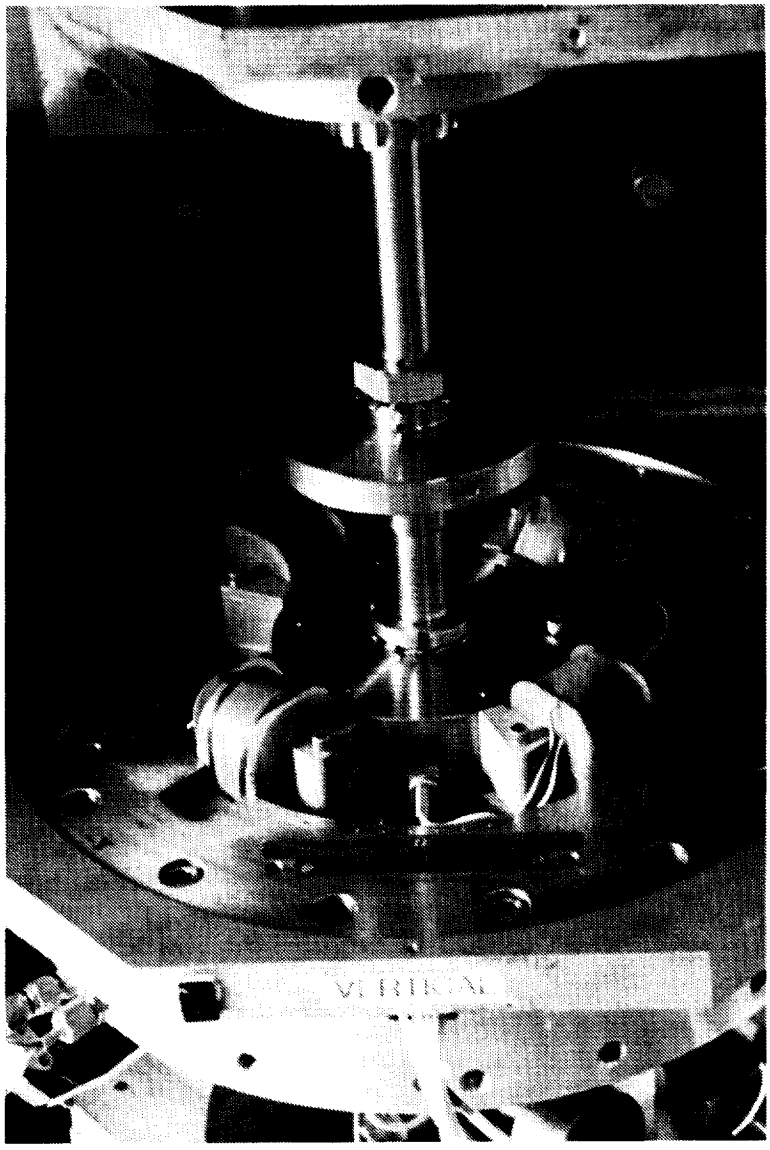

Figure 1-5. Magnetic Bearing Shaft, Flywheel, Force Generators

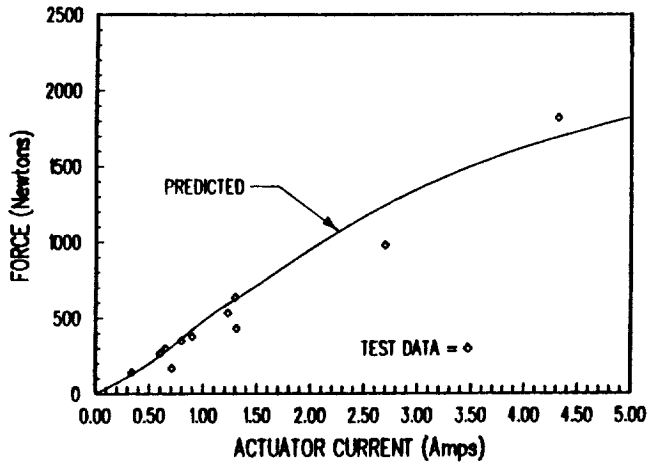

Figure 1-6. Load Output Vs. Actuator Input Current

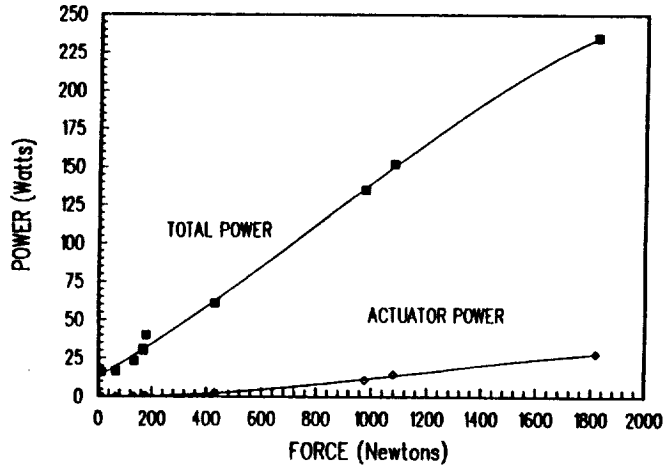

Figure 1-7. Magnetic Bearing System Power Consumption Vs. Load

The CMBTF design and test results confirm the analytical predictions. Magnetic bearings can, indeed, be considered for applications in hostile environments, even when such applications are size, weight, and power draw sensitive.

The detailed analyses, design, fabrication, assembly, and tests carried out on this program are discussed in the following sections.

2.0 SELECTION OF MAGNETIC BEARING TYPE

2.1 Literature/Industry Survey

A very complete literature survey of magnetic bearing technology was made. Sources surveyed for reports included the University of Southern California library, DTIC, NTIS, NASA Industrial Applications Center, trade journals, proceedings of professional society meetings, and discussions with experts in industry and universities doing research on magnetic bearings. Over 650 reports were identified during the literature survey; and the most applicable 650 reports were identified during the literature sruvey; and the most applicable references are included in Section 8.0. The industry/commercial references, where applicable, are mentioned in the trade-off study, the analyses, or the detailed design. The literature survey revealed that during the last 25 years, magnetic bearings have progressed from laboratory curiosity to very specialized, sophisticated applications such as spacecraft mechanisms, to more conventional machines such as compressor and machine tool spindles.

Magnetic levitation has been a topic of serious engineering interest for 150 years. However, the realization of potential advantages offered by magnetic bearing technology escaped scientists and designers until three important, relatively recent developments were made:

1. Advancements in high energy product permanent magnet materials;

2. Development of high-saturation flux ferromagnetic materials, and;

3. Development of integrated circuit solid-state micro-electronics.

These developments have lifted the most significant barriers to application of magnetic suspension to a multitude of modern machines. Magnetic bearings offer the advantages of very long life and high reliability by (1) the elimination of wear-out and fatigue failure modes, (2) elimination of a lubrication supply and circulation system, and (3) providing a way to avoid the single-point failure limitation of conventional bearing designs. The very low rotational axis torques of magnetic bearings make possible lower bearing power loss, higher accuracy pointing systems, high resolution instruments, and improved rotor dynamics for pumps.

The literature survey was used to categorize all types of magnetic bearings and to identify those types which were relevant to the CMBTF project. The relevant types were used to configure candidate designs for the trade-off

study. The literature survey and industry survey were used to identify state-of-the-art magnetic materials. The industry survey was also used to identify state-of-the-art commercial embodiments of magnetic bearings for the concept trade-offs.

Key characteristics to be considered for the literature/industry survey and the subsequent trade-off study were:

1. magnetic circuit type
2. magnetic material
3. rotor material
4. electromagnet coils (size, core material, cladding/insulation)
5. servo control system (analog vs. digital as well as control iaw type)
6. position sensor type

The literature survey was most beneficial with respect to identifying magnetic circuit types and servo control system concepts, and in identifying commercially available magnetic materials, rotor materials, electromagnet materials, and position sensors. However, because of the near term application of the CMBTF, we found it necessary to perform the magnetic circuit type trade-off by using commercially available magnetic bearings (see Section 2.2). The magnetic circuit type review described in Section 1.0 does, however, include all relevant magnetic circuit types found in the literature.

2.2 Trade-off Study

The concepts, approaches, and implementations found during the literature/industry survey were used to design various configurations which could meet the system requirements described earlier. The configurations, based on the various magnetic bearing concepts, were evaluated based on system size, weight, and power draw.

The design characteristics, based on the literature/industry survey, included:

1. Magnetic circuit type
   - electromagnet-bias/electromagnetic-control vs. permanent-magnet-bias/electromagnetic-control
   - heteropolar vs. homopolar design

2. Magnetic material
   - high energy product of permanent magnets
   - high linearity of "soft" magnetic material
   - high saturation flux of "soft" magnetic materials

3. Rotor material
   - magnetic at room and cryogenic temperatures
   - high strength at room and cryogenic temperatures
   - high saturation flux density

4. Electromagnet coils
   - suitable size (for number of windings required), material, and composition to provide the desired electromotive force at room and cryogenic temperatures

5. Servo control system
   - analog vs. digital
   - proportional - derivative
   - proportional - integral - derivative

6. Position sensors
   - suitable sensitivity and linearity
   - sufficiently low crosstalk among measurement channels
   - high signal to noise ratio

The magnetic-circuit type is the dominant characteristic in determining the size, weight, and power draw of a magnetic bearing design. Also, the magnet-circuit type limits the maximum safe or operational RPM of a magnetic bearing by virtue of eddy current/hysteresis heating effects.

The approach used to select the best design approach for the CMBTF was to first establish a set of requirements typical of small pumps. Four types of magnetic bearings were compared for size, weight, and power consumption.

Magnetic bearing design is a highly heuristic process; and there are always trade-offs between size, weight, and power consumption. However, by using the same materials, coil power density, and magnetic materials design limits (flux, coercive strength, and magnetic induction), an objective comparison of the relative merits of each design can be made. Table 2-1 depicts the trade-offs that led to selecting the magnetic bearing design for incorporation in the CMBTF.

Design Characteristic	Preferred Candidate	Remarks
Magnetic Circuit Type	Homopolar, Permanent Magnet Bias/ Electromagnet Control	Lowest size, weight, power draw, eddy current/hysteresis loss
Magnetic Material (laminations on stator and rotor)	Vanadium Permendure	High energy product, adequate linearity at the operating point, adequate structural properties, adequate room and cryogenic temperature performance
Shaft Material	CRES 416	Suitable magnetic and structural properties at room and cryogenic temperatures
Electromagnetic Coils	Copper	Meets amp-turns requirements at cryogenic temperatures, adequate performance at room temperature, commercially available
Servo Control System	Analog PD	Meets requirements near term, commercially available components, minimum development required
Position Sensors	Eddy current	Low cost, meets requirement

TABLE 2-1. Magnetic Bearing Type Trade-off Study

3.0 MAGNETIC BEARING SYSTEM ANALYSIS

3.1 Dynamic Analysis

Note: The design calculations shown in this report are the original calculations. Changes made during the fabrication of hardware are not reflected herein.

3.1.1 Rotor Finite Element Dynamic Model

The rotor system can be modeled as a finite element model as shown in Figure 3-1:

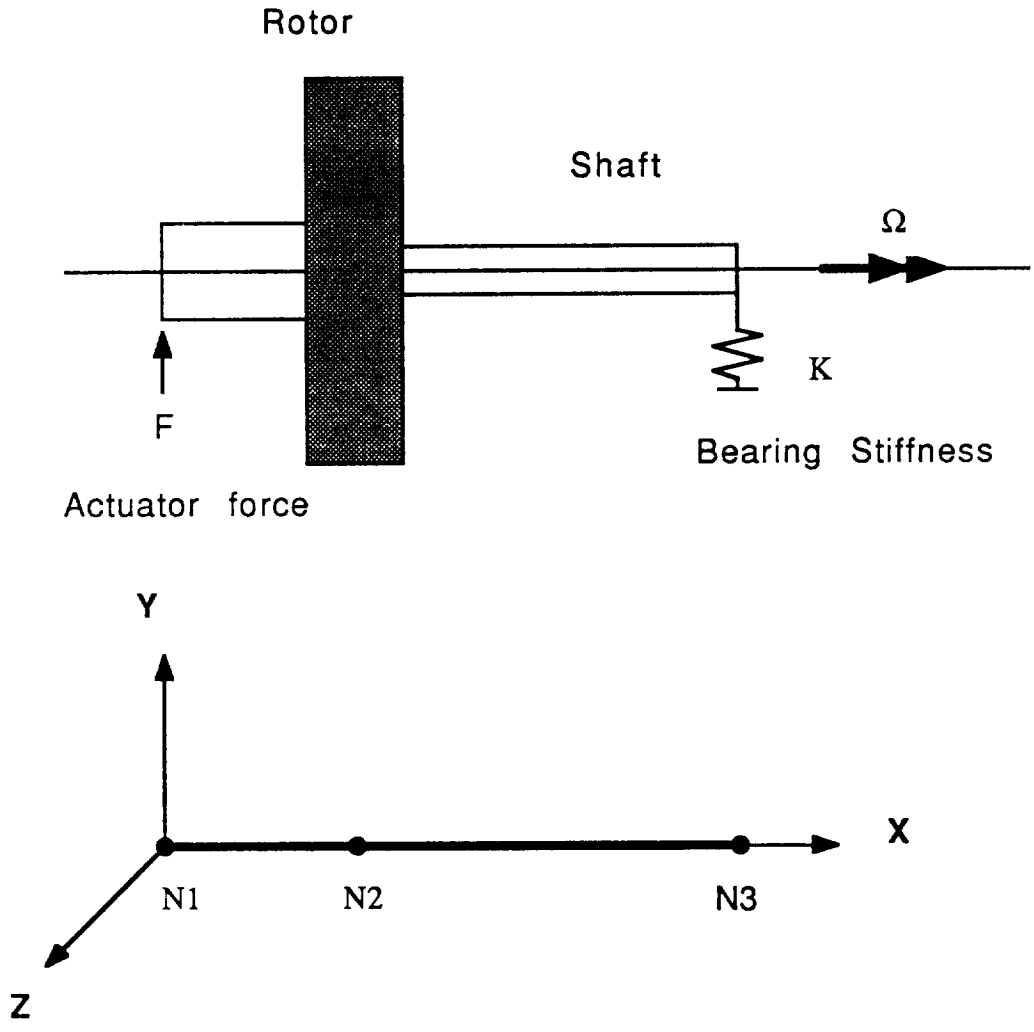

Figure 3-1. Rotor Finite Element Model

All displacements δ are measured in the rotating system spinning at speed Ω about the X axis (rad/sec units). The defining equation is:

$$[M]\ddot{\delta} + [D]\dot{\delta} + [K]\delta = f$$

where:

$$[D] = [D_R] + 2\,\Omega\,[G]$$

$$[K] = [K_R] + \Omega^2\,[C]$$

$$f = f_R + \Omega^2\,s$$

The displacement vector δ is of size 6X NGRID where NGRID is the number of grid points in the model. Each grid point has six degrees of freedom - three translation and three rotational. The X direction lies along the spin axis. The spin rate is Ω. The matrices **M**, $\mathbf{D_R}$, **G**, $\mathbf{K_R}$, and **C** are all time invariant matrices. **M** is the system mass matrix. $\mathbf{D_R}$ is the system damping matrix (non-gyroscopic). **G** is the gyroscopic damping matrix related to the spin dynamics. $\mathbf{K_R}$ is the system stiffness matrix related to the centrifugal effects of the spinning system. The vector $\mathbf{f_R}$ is the external force applied to the system (servo control) applied in the rotating frame. The vector **s** is a static force vector representing the cg offsets in the system. Note that all displacements and forces are measured with respect to the rotating frame and not to inertial reference. The inertial displacements Δ_Y and Δ_Z can be calculated from the local frame displacements δ at any specific time **t** by,

$$\Delta_Y = \cos(\Omega t)\,\delta_Y - \sin(\Omega t)\,\delta_Z$$

$$\Delta_Z = \sin(\Omega t)\,\delta_Y + \cos(\Omega t)\,\delta_Z$$

Similarly, the external forces (such as control forces) $\mathbf{F_Y}$ and $\mathbf{F_Z}$ can be transformed from the inertial frame into the rotating frame using the following inverse transformation:

$$f_Y = \cos(\Omega t)\,F_Y - \sin(\Omega t)\,F_Z$$

$$f_Z = \sin(\Omega t)\,F_Y + \cos(\Omega t)\,F_Z$$

3.1.2 Output Format

The matrix file has the following format:

TITLE:	title of analysis
MATRIX SIZE:	size of matrices = 6 X (number of grid points)
MATRIX:	matrix name
a1, a2, a3, ...	matrix elements

The matrices are output by rows in the following format:

```
      DO 100 I=1 ,NGG
  100 WRITE (2,6000) (AMAT(I,J) ,J=1 ,NGG)
 6000 FORMAT (1P5E16.6)
```

The vectors are written similarly. Several rotor configurations were evaluated before the shaft geometry shown in Figure 3-2 was selected for the CMBTF.

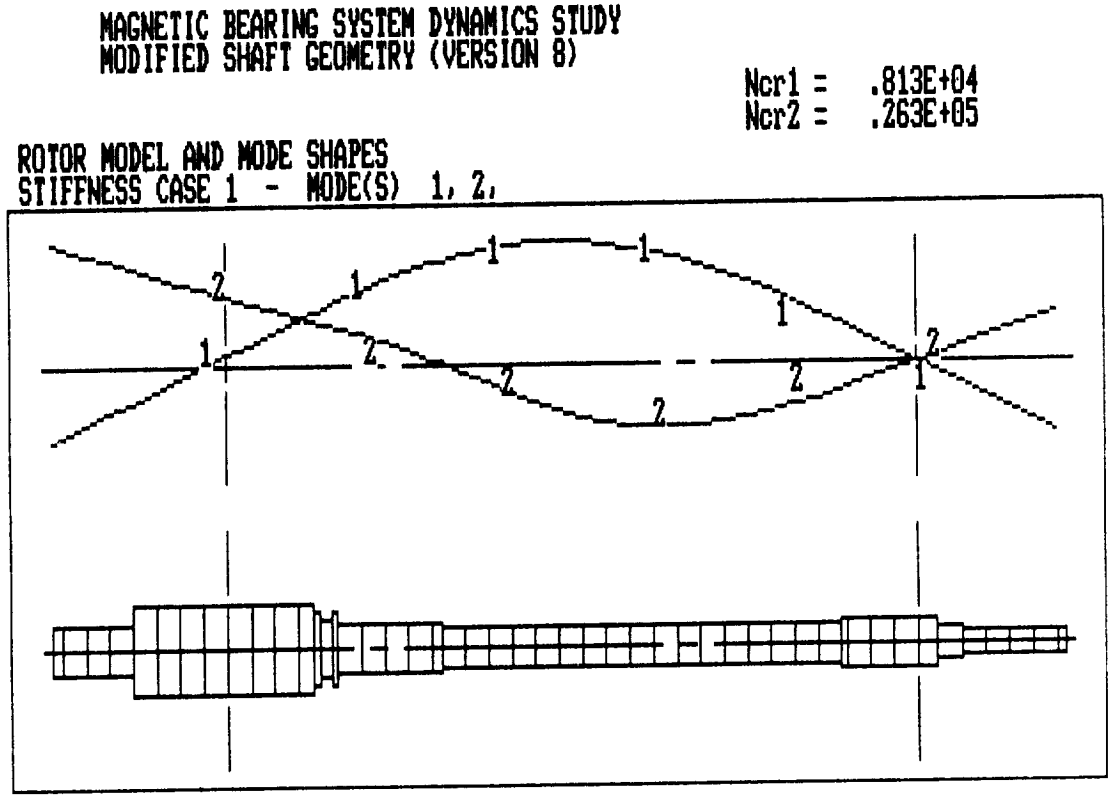

Figure 3-2. Modified Shaft Geometry, Version 8

where the bearing stiffness is:

Mode 1 = 1.75×10^5 lb/in.

Mode 2 = 1.75×10^5 lb/in.

3.2 Magnetic Analysis

The design calculations in this section are the result of a number of iterations that were required to meet all of the design requirements. These requirements were:

1. Outer bearing diameter: minimum practical size.

2. Gap diameter at rotor 3.0"

3. Gap width: 0.015" (original design)
   0.024" (actual hardware)

4. Maximum allowable magnetic induction in the Vanadium-Permendure core not to exceed 16 kGauss in order to maintain a linear-force/current relationship of the control coils.

5. Effective force of both the permanent magnet and the control coils in either the X or Y direction to be 500 lb. for the assembly.

The method of calculation requires two steps: 1) define the permanent magnet characteristics, and 2) define the electromagnet characteristics. The first step determines the dimensions of the permanent magnet and its circuit (consisting of the poles, air gap, and shaft) within the design envelope indicated above. The second step determines the control coil dimensions and electrical characteristics required to offset the attraction forces at the poles by the permanent magnet.

The intrinsic magnetic properties of Samarium-Cobalt material for the permanent magnet are assumed to increase by 45% at liquid Nitrogen temperature (-320° F) versus the normal operating temperature (70° F). The values at 70° F are: B_0 = 11 kilo Gauss, and H_0 = 10.3 kilo Oersted. No data is available for SmCo magnetic properties at -320° F; but in some of the manufacturers' literature, the above values are shown to increase by 20 to 25% at an operating temperature of 0° F. Therefore, the 45% increase used here may be somewhat conservative. The units used in the calculations are:

Magnetic induction:	kilo Gauss	(kG)
Magnetic flux:	kilo Maxwell	(kMx)
Magneto Motive Force:	Ampere windings	(Aw.)

All dimensions are in inches. The permeability of free space (u_0) is 0.0032 kMx/Aw/inch.

3.2.1 Requirements Analysis

The desired radial force for the assembly is 500 pounds. The number of poles on either side of the assembly is four (4). The net design force on each lamination stack is 250 pounds in either the X or Y direction.

The total number of wire slots for the coils on the circumference of the stator is 16 (4 per pole).

The pole area material reduction due to the coil slots is 17% of the circumference.

The gap diameter is 3.0". The gap distance when the shaft and stator are concentric is .024". Therefore, the stator pole diameter is 3.048" (3+.024+.024).

The coil slot width is 0.11"; slot height is 0.18".

The cross-sectional area available for installation of the electromagnetic control coil is:

control coil area = (2 slots)(width)(height)

= (2)(0.11)(0.18)

= 0.04 sq. inch

pole length = 1.2 inches

The material cross-section of each pole equals:

pole area = (pole circumference)(100%- pole reduction due to slots)(pole length) / number of poles

$$= \frac{(3.048\ \pi)(83\%)(1.2")}{4}$$

= 2.38 sq. inch.

3.2.2 Permanent Magnet Circuit Calculations

(a) The radial force per opposing pole pair at each side of the assembly is 500/2 = 250 lb. net. Due to the staggering of coils in the slots of each pole, the arc adjusted factor equals:

$$f_r = (a)(R) / 2R \sin\frac{a}{2}$$

$$= \frac{a}{\left[2 \sin\frac{a}{2}\right]}$$

where:

$$a = \frac{\pi}{2} \quad \text{(for 4 poles)}$$

so that:

$$f_r = 1.11.$$

The gross force per pole is:

$$F = (1.11)(250)$$

$$= 277 \text{ lb. gross.}$$

(b) The following properties of SmCo permanent magnet (P.M.) at liquid Nitrogen temperature were used in the calculation:

B_o = 145% of 11 (magnetic induction)
= 16 kG;

H_o = 145% of 10.3 (magnetic intensity)
= 15 kOe;

u_m = B_o/H_o (relative permeance)
= 16/15
= 1.07

(c) It is assumed that the flux leakage at the permanent magnet and fringing at the air gaps is 25%.

(d) An estimate of the required magnetic induction at the air gap that meets the 277 lb. attraction force can be made by ignoring the reluctance of iron (since the air gap reluctance is assumed dominant in this preliminary calculation).

The attraction force in the air gap at the poles is:

$$F = (0.58)(B^2)(A) \quad \text{(lb.)}$$

where:

B = magnetic induction (kG)

A = pole area (sq. inch)

so that:

$$B = \sqrt{\frac{F}{0.58\,A}}$$

$$= \sqrt{\frac{277}{(0.58)(2.38)}}$$

$$= 14.2 \text{ kG}$$

The magnetic flux ϕ of the P.M. (per 1/4 of its circumference) is:

$$\phi = (B)(A)$$

$$= (14.2)(2.38)$$

$$= (33.65 \text{ kG})(6.45)$$

$$= 217 \text{ kMx}$$

The net magnetic flux is:

$$\phi_{pm} = (4)(217)$$

$$= 868 \text{ kMx}$$

(e) With the above values and assumptions, the stator height at the narrowest diameter of the transition piece between the permanent magnet and the poles can be calculated as follows:

The maximum allowable magnetic induction is 16kG. The outside diameter of the permanent magnet is 5.0".

The area at the narrowest diameter of the stator is:

$$A_{st} = \frac{\phi_{pm}}{6.45\ B_{max}}$$

$$= \frac{868}{103.2}$$

$$= 8.41 \text{ (add 14\% for leakage)}$$

$$= 9.52 \text{ sq. inch} \quad \text{(2.38 sq. inch per 1/4 of the circumference)}$$

Therefore, the stator height is $\frac{9.52}{5\,\pi} = 0.61"$.

(f) In determining the physical dimensions of the permanent magnet, an iterative procedure was used that minimized the bearing envelope within the design requirements described above. The dimensions of the permanent magnet were determined by the procedure to be:

magnet outside diameter	5.0"
magnet inside diameter	3.3"
magnet width	0.35"

(g) The internal reluctance of the permanent magnet is determined from the equation:

$$R_m = 1_m / (u_o)(u_m)(A_m)$$

where:

R_m = magnet reluctance (Aw/kMx)

l_m = magnet width (inches)

u_o = permeance in space
= 0.0032 kMx/Aw

u_m = relative permeance of the magnet
= 1.07

A_m = cross-sectional area of the magnet
= 2.77 in.^{2}

so that:

R_m = 0.35 / (0.0032)(1.07)(2.77)
= 37 Aw/kMx

(h) Now that the magnet reluctance and all physical dimensions in the permanent magnet circuit are determined, the actual magnetic properties based on the variable operating point of the magnet and the variable external reluctances can be finalized. These properties are shown in Table 3-1.

Part Name	Area (sq. in.)	Flux Length (inches)	Magnet Induct. (kG)	Magnet. flux (kMx)	Relative Permeance (u_r)	Reluct. Aw/kMx
Permanent Magnet (1/4 circumference)	note 1. 2.77	.35	note 2. 11.19	200	1.07	37.01
Stator at poles	2.38	.99	13.01	200	3116	.04
Cyl sec's at poles	2.38	1.20	13.01	200	3116	.05
Radial at 2 poles	2.38	1.26	13.08	200	3040	.05
Air Gap 2 places	2.16	.03	14.33	200	1.00	4.33
Rotor Shaft	2.05	2.54	15.13	200	553 note 3.	0.70
Total External Reluctance						5.17

TABLE 3-1. Permanent Magnet Flux Table.

Notes:

1. One quarter of the magnet cross-section
2. 25% leakage or fringing allowed (gross inductance is 16 kG max.)
3. Nearing saturation

The net magnetic induction in the above table, at the operating point of the permanent magnet, is calculated from the equation:

$$B_{op} = \text{P.M. operating point (kG)}$$

$$= \frac{B_o \text{ net}}{\left(\frac{1 + R_{ex}}{R_m}\right)}$$

$$= \frac{(16)(0.75)}{\left(\frac{1 + 5.17}{37}\right)}$$

$$= \frac{71.96 \text{ kMx}}{6.45}$$

$$= 11.2 \text{ kG}$$

where:

B_o net = net intrinsic magnetic induction of P.M.

= 16 kG - 25% fringing loss

R_{ex} = external reluctance of P.M. circuit (Aw/kMx)

R_m = internal reluctance of P.M. (Aw/kMx)

(i) The attraction force of each of these 8 poles on the shaft due to the P.M. alone is:

$$F = (0.58)(B_{gap}^2)(A_{gap})$$

$$= (0.58)(14.3^2)(2.163)$$

$$= 256 \text{ lb.}$$

Since the shaft is assumed to be perfectly concentric with the pole stator the resultant rotor force theoretically equals zero.

3.2.3 Electromagnetic Coil Calculations

(a) The total cross-sectional area for each pole core, as previously calculated, is 0.038 sq. inch.

The American Wire Gauge number used is 26 AWG enamel covered copper wire, with a diameter of 17.3 mils including the enamel.

Bare wire cross-sectional area is 252 circular mils.

With a wire slot fill factor of 0.9, the number of windings per coil are:

$$n = \frac{(0.038)(0.9)}{0.0173^2}$$

$$= 115 \text{ windings.}$$

The average length of each coil winding is 1/4 the circumference at the pole gap diameter + 2 times the pole length, or:

$$l_{av} = \left[\frac{3.048\,\pi}{4}\right] + (2)(1.2)$$

$$= 4.79"$$

The total wire length per coil is (4.79)(115) = 551".

(b) The resistivity ratio of copper at liquid Nitrogen temperature (77° Kelvin) versus 273° K (0° C) is obtained from a number of investigators and summarized as follows:

Powell et. al. (1959)	=	0.123
Dominicali and Christenson	=	0.130
Pawler and Rogalio	=	0.122
Average	=	0.125

In the equation for the resistivity of copper at cryogenic temperatures, the average value is used.

The resistivity curve is practically a straight line sloping at 45° in the temperature range of 77° K to 300° K; meaning the resistivity ratio is linear with temperature in that range.

Based on the above information, the relative resistivity equation converted to degrees F is given by:

$$R_t = (R_{70})(0.839 + (0.002297)(t))$$

where:

t = wire temperature (° F)

The copper wire resistance at room temperature (70° F) is:

$$R_{70} = (0.86)(l/a) \text{ (Ohm)}$$

where:

l = wire length

Therefore, the resistance equation over the -320 to 200° F temperature range becomes:

$$R_t = (0.86)(l/a)(0.839+(0.002297)(t)) \quad \text{(ohm)}$$

where:

l	=	wire length	(inches)
a	=	bare wire cross-section	(circ. mil, 10^{-6} in.^{2})
t	=	operating temperature of the wire	(° F)

The coil resistance at -290° F (allowing for 30° F temperature rise during operation) is:

$$R_{coil} = (0.86)\left[\frac{551}{252}\right](0.839 + (0.002297)(-290))$$

$$= 0.33 \text{ ohm} \quad \text{(versus 1.88 ohm at 70° F)}$$

(c) The reluctance of the flux path for the two coils positioned at opposite sides of the rotor and operating in cooperation with each other is practically equal to the value shown in the flux table:

2 air gaps	=	4.33 Aw/kMx
poles, shaft,and stator housing	=	0.75 Aw/kMx
reluctance	=	5.08 Aw/kMx
reluctance per coil	=	5.08/2
	=	2.54 Aw/kMx

The self-inductance L of a magnetic coil is calculated from:

$$L = \frac{\left[\frac{n^2}{Rl_c}\right]}{10^5}$$

where:

L	=	inductance (Henry)
Rl_c	=	coil reluctance (Aw/kMx)
n	=	number of windings of the coil

So that:

$$L = \frac{\left[\frac{115^2}{2.54}\right]}{10^5}$$

$$= 0.052 \text{ henry}$$

The time constant **T** is given by:

$$T = L / R$$

$$= \frac{0.052}{0.33}$$

$$= 158 \text{ msec. (at } -290^{\circ} \text{ F)}$$

(d) Calculation of the coil Ampere-windings (Aw) required to offset an effective permanent magnet force **F**:

The forces due to the magnetic fluxes ϕ_{pm} of the permanent magnet are in equilibrium at the air gap as long as the rotor is concentric with the poles.

The force exerted by one pole on the rotor is:

$$F = \phi_{pm}^2 / 72.4 / A_p$$

where:

F = attraction force on the rotor (lb.)

ϕ_{pm} = permanent magnetic flux (kMx)

A_p = pole area (sq. inch)

An additional magnetic flux (ϕ_c) by the control coils at the stator poles strengthens the flux on one side and weakens the flux on the other side of the rotor.

The resultant control force thus becomes:

$$F_c = \frac{(\phi_{pm} + \phi_c)^2 - (\phi_{pm} - \phi_c)^2}{\left[\frac{72.4}{A_p}\right]}$$

After rearranging and solving for ϕ_c, the result is:

$$\phi_c = \frac{(72.4)(Fc)(Ap)}{\left[\frac{4}{\phi_{pm}}\right]}$$

The number of the Ampere windings for each control coil is:

$$NI_c = (\phi_c)(R_c)$$

Eliminating the ϕ_c from the last two equations yields:

$$NI_c = \frac{(18.1)(F_c)(A_p)(R_c)}{\phi_{pm}}$$

where:

NI_c = the number of Aw. for each coil

F_c = resultant coil force (lb.)

A_p = pole area (sq. inch)

R_c = coil reluctance (Aw/kMx)

ϕ_{pm} = permanent magnet flux (kMx)

so that:

$$NI_c = \frac{(18.1)(277)(2.38)(2.54)}{200}$$

$$= 152 \text{ Aw}$$

The heat dissipation per coil operating at liquid Nitrogen temperature is:

$$W = (I^2)(R)$$

$$= (1.3^2)(0.33)$$

$$= 0.56 \text{ Watt}$$

With 4 coils active in either the X or Y direction, the total heat dissipation is:

$$= (4)(0.56)$$

$$= 2.2 \text{ Watts.}$$

3.2.4 Performance Analysis of Cryogenic Bearing at Room Temperature

(a) Permanent Magnet

At room temperature (70° F), the total magnetic flux is 138 kMx, compared with 200 kMx at -320° F (see Table 3-1). The magnetic induction at the air gap equals 11 kG. (compared to 14.3 kG at cryogenic temperatures).

The attraction force equals:

$$F = (0.58)(B^2)(A)$$

$$= (0.58)(11^2)(2.38)$$

$$= 166 \text{ pounds}$$

(b) Electromagnetic Magnet

The self-inductance of the coil is a function of the reluctance of the coil circuit and the number of coil windings. Both of these remain constant with temperature; so the self-inductance of the coil remains 0.052 Henry.

As calculated earlier, the coil resistance at room temperature is 1.88 Ω; so the time constant at room temperature is 0.052 / 1.88 = 28 msec.

The maximum allowable current density at room temperature is 3 mA/circular mil (compared to 5 mA). The resulting Magneto Motive Force of the coil is (3/5/1.45)(277) = 115 lb.

The permanent magnet and electromagnet are well matched, but the system produces less than half the radial force at room temperature that will be produced at cryogenic temperatures.

3.3 Ball Bearing Analysis

Analysis of Upper Bearing Loads

The shaft upper end bearing loads are due to (1) preload, (2) rotor weight, and (3) drive belt pulley loads. The pulley loads were determined empirically by measuring the ECDR idler pulley-to-belt load, then calculating the bearing component from the geometry of the pulley/drive system. The pulley/drive system is shown schematically in Figure 3-3, as viewed from the top of the test fixture.

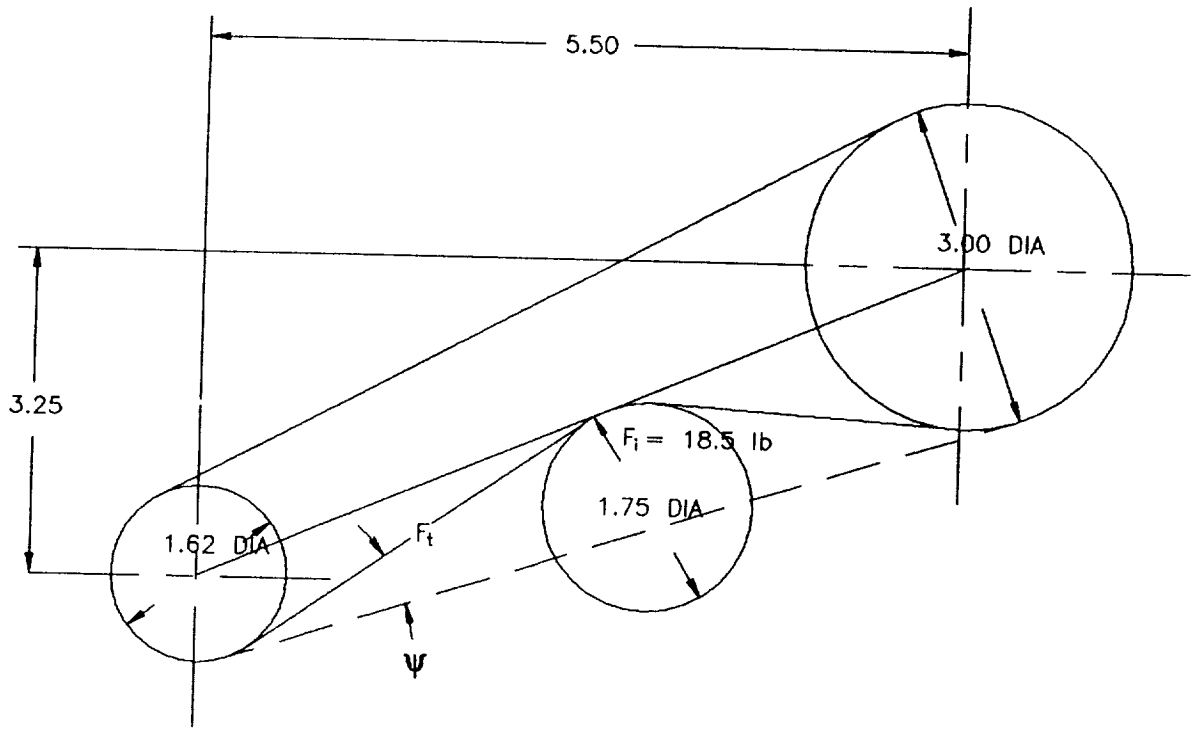

Figure 3-3. ECDR Drive Belt & Pulley Geometry, Viewed From Above

Belt tension was determined by loosening the hold-down screw that secured the ECDR idler pulley, as delivered, and measuring the force required to maintain the idler pulley in the normal running position. The idler pulley force was measured with a Wagner model FD 127 force gauge. The measured force was 18.5 pounds. From Figure 3-3:

$$\sin \psi = \frac{0.875}{2.75}$$

$$\psi = 18.55 \text{ degrees.}$$

An analysis of stiffness and lube factors for the top touchdown bearings (code NASATOP) is shown in Figure 3-4 and 4-5.

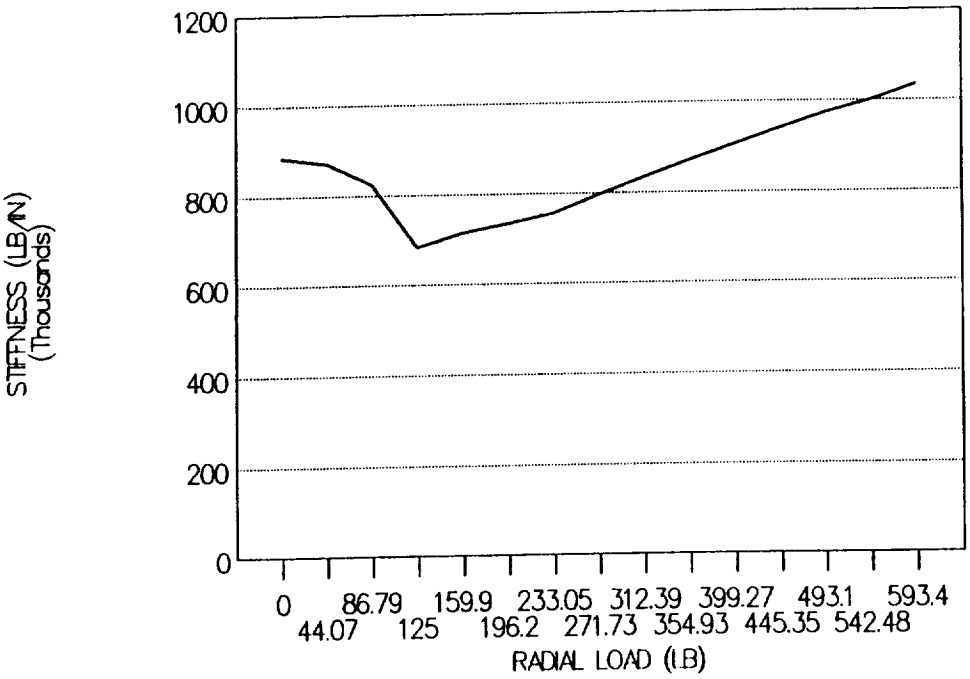

Figure 3-4. Stiffness Vs. Radial Load

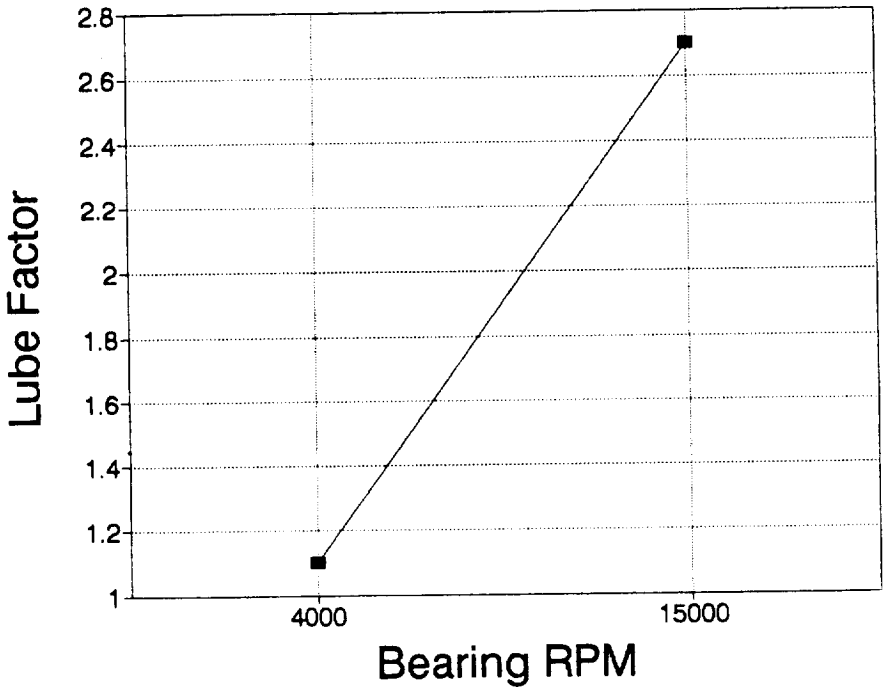

Figure 3-5. Upper Bearing Lube Factor Vs. RPM

This is the steady state force on the upper bearing due to tension on the drive belt. The upper bearing will also have a variable radial load due to the force generator acting on the rotor inertial mass. These forces are shown in Figure 3-6:

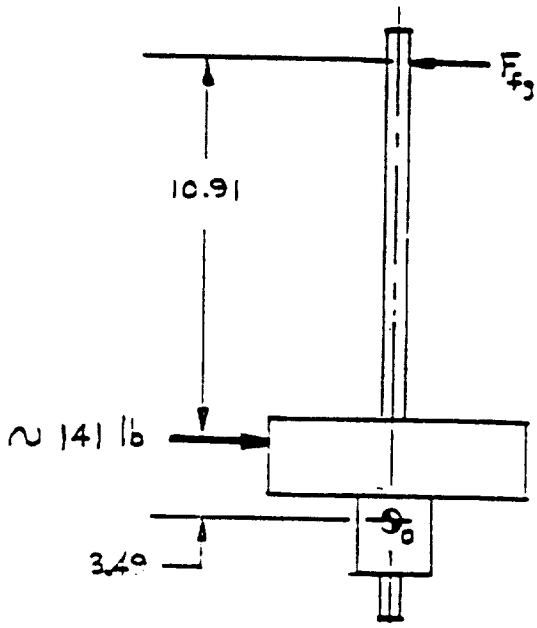

Figure 3-6. Forces Acting on the Rotor That Affect Upper Bearing Load

From Figure 3-6, we can sum moments about the rotor center of mass (point 0):

ΣM_0	=	0
141(3.49) - F (14.4)	=	0
F_{fb}	=	34.2 lb. cyclically varying load

These load components were used in analyzing the upper bearing stresses and fatigue life.

The results of the lower touchdown bearing analysis (code NASABOT) are summarized in Tables 3-2 and 3-3.

LOAD/DEFLECTIONS SUMMARY, DUPLEX BEARING:	
Radial Load	163 lbs
Deflection	204.3 micro inches
Axial Load	0 lbs
Deflection	0 micro inches
Moment Load	0 inch lbs
Angular Rotation due to Applied Moment	0 arc seconds
Preload	18.498 lbs
Max Mean Bearing Stress	159.5 KS
Max Contact Angle	13.41 degrees
Max Ball Load (on ball 1, row 1)	36.19 lbs
Average Ball Load	13.46 lbs
Row 1, Number of Loaded Balls	7 (77%)
Row 2, Number of Loaded Balls	7 (77%)
The Bearing Configuration is non-rigid	

Table 3-2. Bottom Bearing Load and Deflections

L10 LIFE AND RELIABILITY CALCULATIONS ARE BASED ON THESE LOADS:			
Radial Load	163 lbs	Axial Load	0 lbs
Moment Load	0 inch lbs	Preload	18.498 lbs
Max Contact Angle	13.41 degrees	Lubricant Factor	1

THE L10 LIFE (HOURS) , WHEN ROTATING AT 1500 RPM:					
For Row 1	5213.09	For Row 2	5213.12	Combined	2793.63

RELIABILITY @ 15000 RPM			
HOURS	ROW 1	ROW 2	COMBINED
10000	80.4706	80.4707	64.7553
5623	89.1710	89.1711	79.5148
3162	94.1332	94.1333	88.6107
1778	96.8611	96.8611	93.8208
1000	98.3318	98.3318	98.2408
562	99.1165	99.1165	99.0681
316	99.5330	99.5330	99.0681
178	99.7534	99.7534	99.5074
100	99.8698	99.8698	99.7398
56	99.9313	99.9313	99.8627
32	99.9638	99.9638	99.9275
18	99.9809	99.9809	99.9618
10	99.9899	99.9899	99.9798

Table 3-3. Bottom Bearing Life and Reliability

3.4 Stress Analysis

Dynamic Stress Analysis for Magnetic Bearing Flywheels

The flywheel is keyed to the main shaft and rotated at the operating shaft speed. The test speed is 15,000 RPM, design speed is 25,000 RPM. The centrifugal effects create dynamic stresses on the flywheel. These effects are analyzed as follows:

Operating Conditions: ω_s = 15,000 RPM to 25,000 RPM
= 1570 rad/sec to 2618 rad/sec

Geometry of the Flywheel: (in inches)

Case 1:	O.D.	=	5
	I.D.	=	1.187
	W	=	1.25
Case 2:	O.D.	=	5.4
	I.D.	=	1.187
	W	=	1.25

Material: AISI 1018

Density = $\frac{0.283 \text{ lb}}{\text{in.}^3}$

Poisson's Ratio = 0.29

Analysis:

The component stresses (σ_r, σ_θ, σ_t) were calculated and the combination of stresses obtained.

A uniform cylinder of uniform thickness outer/radius R in. and density $\frac{\delta \text{ lb}}{\text{in.}^3}$, with a central hole of radius R_0 in., rotates about its own axis with a uniform angular velocity of ω rad/sec.

At any point with a distance r in from the center, there is a radial tensile internal stress and a tangential tensile inertial stress. The maximum radial stress, δ_r, occurs at $r = \sqrt{RR_0}$, and is:

$$\text{Max } \delta_r = \left[\frac{3+\upsilon}{8}\right] \left[\frac{\delta \omega^2}{386.4}\right] (R - R_0)^2 \text{ lb/in}^2$$

The maximum tensile stress, δ_t, occurs at $r = R_0$ and is:

$$\text{Max } \delta_t = \left(\frac{1}{4}\right)\left(\frac{\delta\,\omega^2}{386.4}\right)[(3+\upsilon)R^2 + (1-\upsilon)\,R_0^{2}] \text{ lb/in}^2$$

Von-Mises stress is calculated for 2 locations, at $r = \sqrt{RR_0}$ and $r = R_0$.

	ω = 15,000 RPM			ω = 25,000 RPM		
Case	δ_r	δ_t	δ_{vm}	δ_r	δ_t	δ_{vm}
$r = \sqrt{RR_0}$	2700	9393	9393	3284	10937	10937
$r = R_0$	7500	26120	26120	9132	30412	30412

Table 3-4. Summary of Dynamic Stress

The fatigue strength of the flywheel material must have a value greater than 45,000 psi (30412)(1.5) for a 50% margin of safety.

Dynamic Stress Analysis of Rotor Laminations

The stress is quite low on the rotor under dynamic effects. Therefore, no critical condition exists under dynamic loading for these operating conditions.

Thermal Stress Analysis

The coefficient of thermal expansion for 304 cres:

$$\alpha_o = 9.6 \left(\frac{\mu \text{ in.}}{\text{in.}\,^{\circ}\text{F}}\right)$$

The coefficient of thermal expansion for 1018 low carbon steel:

$$\alpha_i = 6.505 \left(\frac{\mu \text{ in.}}{\text{in.}\,^{\circ}\text{F}}\right)$$

The change in diameter at the interface due to thermal expansion is:

$$
\begin{aligned}
|\Delta D| &= D\,|\Delta T|\,(\alpha_o - \alpha_i) \\
&= (5.25)(70+321^\circ\,F)(9.6 - 6.505)\left[\frac{10^{-6}}{^\circ F}\right] \\
&= (6.35)(10^{-3})\ \text{in.}
\end{aligned}
$$

The shrink-fit pressure is 5147 p.s.i.

The principal stress for the inner component is -0.532×10^4 p.s.i.

The principal stress for the outer component is 1.5762×10^4 p.s.i.

Yield strength for 304 cres is 80×10^3 p.s.i.

Yield strength for 1018 low carbon steel is 48×10^3 p.s.i.

Conclusion:

1. The 1018 steel inner hollow cylinder will fail at operating temperatures below -321° F. The 304 steel outer hollow cylinder can be considered safe for this operating condition.

2. A titanium shell must be inserted between the 304 stainless steel and the 1018 low carbon steel such that the interface between the titanium and the 1018 steel shell will be line-to-line contact under the thermal effect of -321° F (cryogenic condition).

3. The thickness of the titanium shell should be 5/8 in. This will provide an interface between the titanium and the 1018 steel of about 1×10^{-4} in.

4. The stress on:

the 304 shell	=	1.2	(S.F.)
the titanium shell	=	16.5	(S.F.)
the 1018 shell	=	zero	

3.5 Thermal Analysis

This section summarizes the bottom touch-down ball bearing duplex set thermal analysis. Because of the resulting interface clearances at operating temperature, it is required that the shaft/outer ring interface clearance fit is equal to 2 mils (0.002") at room temperature. After cool-down to liquid Nitrogen temperature, the housing/outer ring interface results in a snug fit (0.00012" clearance).

**** INPUTDATA FILE : BOTBRO

Bearing Bore	=	1.0	
Bearing o.d.	=	1.879	
Inner Ring Land o.d.	=	1.3	
Outer Ring Land i.d.	=	1.55	
Number of Balls	=	9	
Ball Diameter	=	0.25	
Inner Ring Curvature	=	0.53	
Outer Ring Curvature	=	0.53	
Init. Cont amg (dgr)	=	25	
Bearing RPM	=	15,000	
Individual Bearing width	=	0.5	
Bearings Inside Spacing	=	0	
Bearings Outside Spacing	=	1	
Thermal coeff			
of Shaft	=	7.2E-06	, 304 St St
of Housing	=	7.2E-06	, 304 St St
of Bearing Rings	=	4.64E-06	, 4400
Shaft Young's Modulus	=	3E+07	
Housing Young's Modulus	=	3E+07	
Shaft Poisson's Ratio			

The Applied Preload	(lb)	=	21.1781	20.0
The Radial Clearance	(micro ")	=	1405.3	1409.2
The Axial Approach	(micro ")	=	216.2 207.9	
The Normal Approach	(micro ")	=	92.6	89.1
Initial Contact Angle	(dgr)	=	25	25.03
The Preload Contact Angle	(dgr)	=	25.74 25.75	
Diam. REDUCTION Inner Ring	(micro ")	=	0	3.3
Diam. INCREASE Outer Ring	(micro ")	=	0	4.4

TEMPERATURE AND FIT EFFECTS OF THE BEARING:

The Shaft/Inner Ring circ. fit	(mils)	=	15
The Housing/Outer Ring circ. fit	(mils)	=	2
The Preload	(lb.)	=	32.8
Radial Clearance	(micro ")	=	1366
Axial Approach	(micro ")	=	302.6
Normal Approach	(micro ")	=	126.7
Act. Initial Contact angle	(dgr)	=	24.25
Operating Contact angle	(dgr)	=	25.26
Max. mean compr. Stress	(ksi)	=	97.9
Hrs of Fatigue Life	(90% Reliab)	=	1.355784E+07
Nut Force on Inner Spacer	(lb.)	=	13024.6
		=	200 (@ 70° F)
Nut Force on Outer Spacer	(lb.)	=	21207.1
		=	200 (@ 70° F)
Shaft/Inner Ring Clearance	(micro ")	=	15992.8
Housing/Outer Ring Clear.	(micro ")	=	120.6
Shaft temp.		=	-320° F
Housing temp.		=	-320° F
Ball Load		=	8.58 lb.

DUPLEX BEARING TORQUE DATA (inch-oz.), (preloaded only):

Rolling Friction	Torque (2 Bearings)	=	2.131	
Duplex Retainer	Drag (2 Bearings)	=	0.0929	
Total Running Friction Torque		=	2.2238	
Viscous Friction Torque at oper. temp.		=	0	
Total Running Viscous + Friction Torque		=	2.2238	(15000 RPM)
Starting or Breakaway Torque		=	3.3357	

3.6 Servo Analysis

A single channel cryogenic magnetic bearing dynamic model, plant and controller, is described. Analysis results of a single channel from the application of a computer program called $Matrix_X$ are presented.

3.6.1 Physical Description

The NASA magnetic bearing incorporates a vertically oriented rotor which is suspended at the top with a mechanical bearing. Rotor position control is provided by dual channel position sensors and a permanent magnetic bias (PMB) electromagnets. These PMB electromagnets provide, in effect, negative springs. The dynamic interaction of the system is the principle topic of this report.

3.6.2 System Models

Plant Models

A mathematical representation of the system is derived with the use of the simplified diagram in figure 3-7:

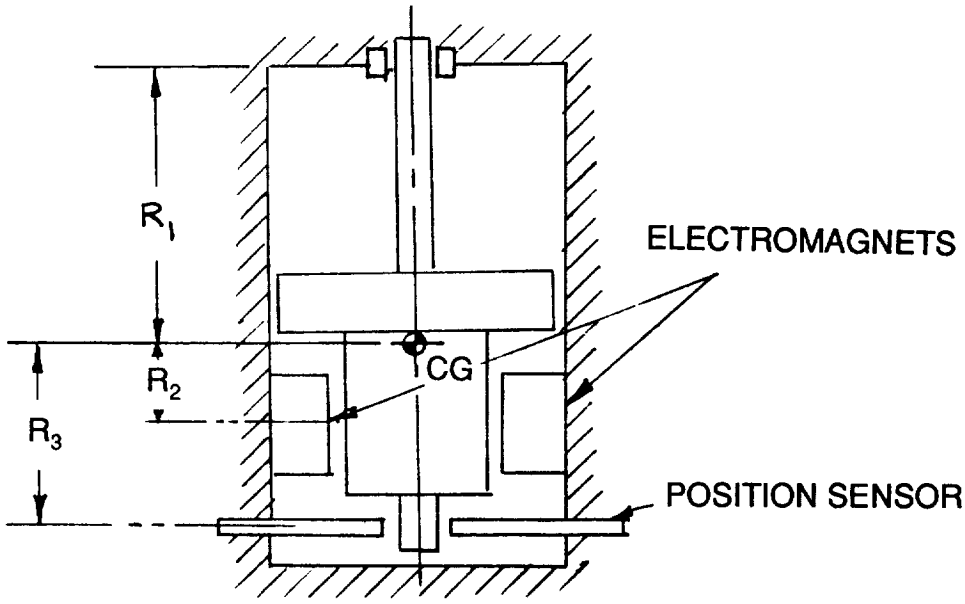

Figure 3-7. Simplified Diagram of System

The mechanical bearing provides translational and rotational spring forces, as well as a certain amount of damping. Electromagnets and position sensors are provided in the two orthogonal axes.

Translational equations are:

$$M\ddot{Y} = F_y - K_1Y + K_2Y - B\dot{Y}$$

and

$$M\ddot{Z} = F_Z - K_1Z + K_2Z - B\dot{Z}$$

where:

K_1 = Translational spring constant provided by mechanical bearing

K_2 = Translational spring constant provided by the magnetic interaction

B = Mechanical bearing damping

F_y = Force of electromagnetic in Y direction

F_Z = Force of electromagnetic in Z direction

The rotational equations are:

$$I\ddot{\theta} = F_y R_2 + \theta R_1^2 K_1 - \theta R_2^2 K_2 + \theta R_3 + I\ddot{\phi}\,\ddot{\psi}$$

and

$$I\ddot{\psi} = F_y R_2 + \psi R_1^2 K_1 - \psi R_2^2 K_2 + \psi R_3 + I\ddot{\phi}\,\ddot{\theta}$$

where:

K_3 = Rotational spring force

$\ddot{\theta}$ = Spin frequency

The "gyro" effect caused by $I\ddot{\phi}\,\ddot{\psi}$ and $I\ddot{\phi}\,\ddot{\theta}$ are the only coupling between the channels. Our analysis ignored this insignificant effect.

Actuator Model

The electromagnets are designed to provide 192 lbs of force per ampere. The actuator includes the motor coil, gain and compensation.

The actuator loop is:

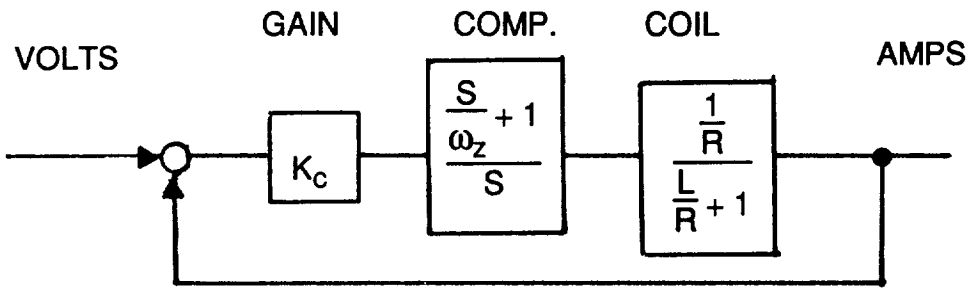

Notch filter

Finite element analyses show the rotor first body bending mode to be 8,130 RPM (850 rad/sec) at bearing stiffness of 1.75×10^5 lb/in. (see Figure 3-2). A notch filter is provided to attenuate disturbances at this frequency. (The attached sample curves are based on an earlier iteration with a first critical of 10,700 RPM.)

Electronic Gain and Compensation

Electronic gain is set to provide a loop stiffness of 200,000 lbs per inch. Compensation is incorporated to provide loop stability. (This stiffness was not actually achieved in preliminary testing.)

3.6.3 Analyses

Notch Filter Design

In order to provide adequate dynamic range at low frequencies and to provide adequate dynamic range for the high frequency actuator, an eighth order notch filter was incorporated. Transfer function of the filter is shown in Figure 3-8. Figure 3-9 represents the Bode plot.

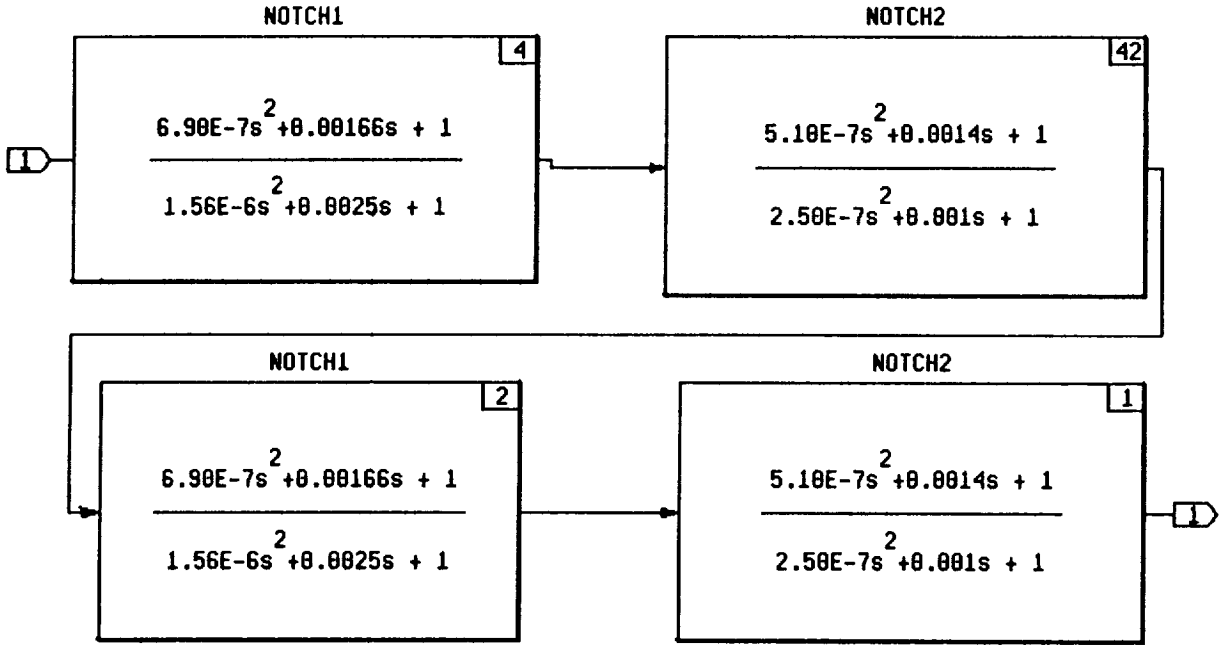

Figure 3-8. Transfer Function of Filter

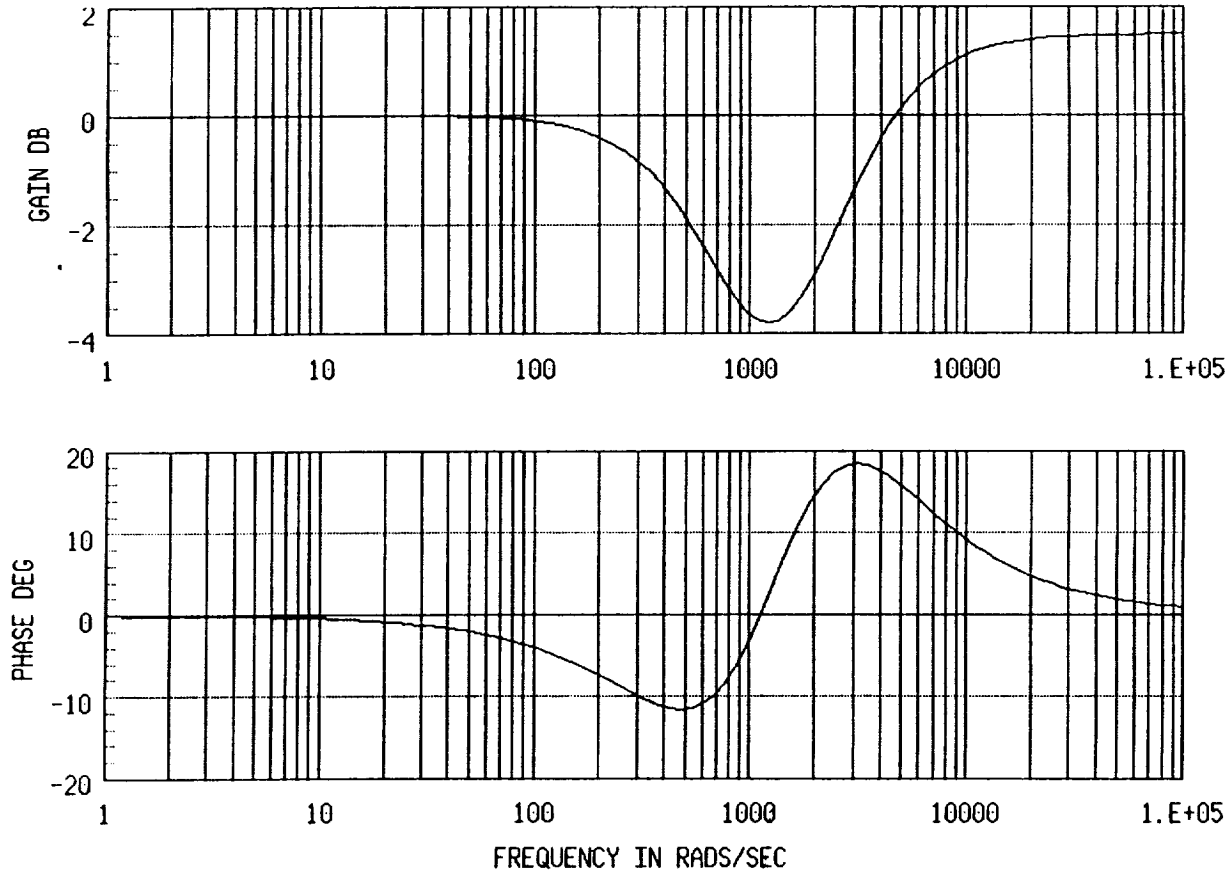

Figure 3-9. Bode Plot

Actuator Design

The actuator gain and compensation was selected to provide critically damped response with a band width of about 5000 rad/sec. Figure 3-10 shows the root locus with specified compensation. As shown, a forward loop gain of 1.28×10^6 provides the desired band-width and damping. The computer model is shown in Figure 3-11.

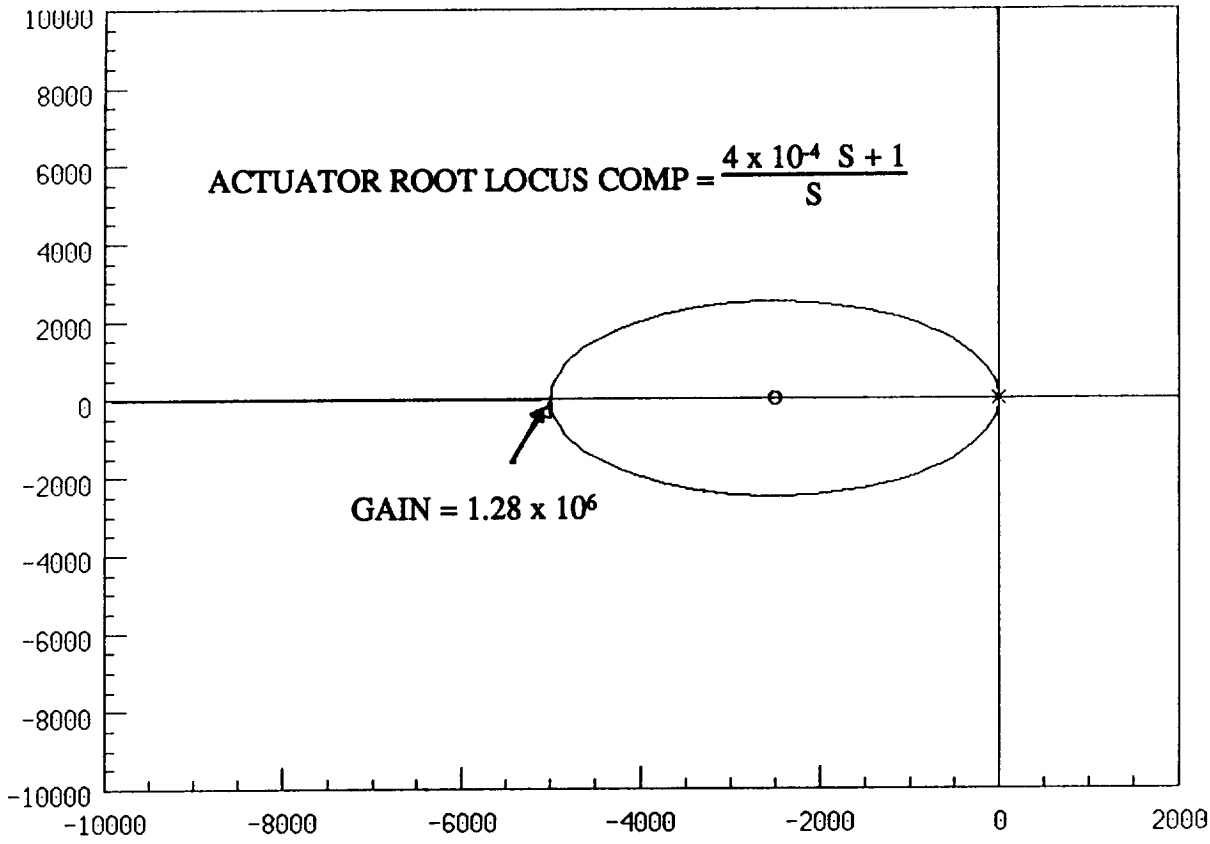

Figure 3-10. Actuator Gain and Compensation

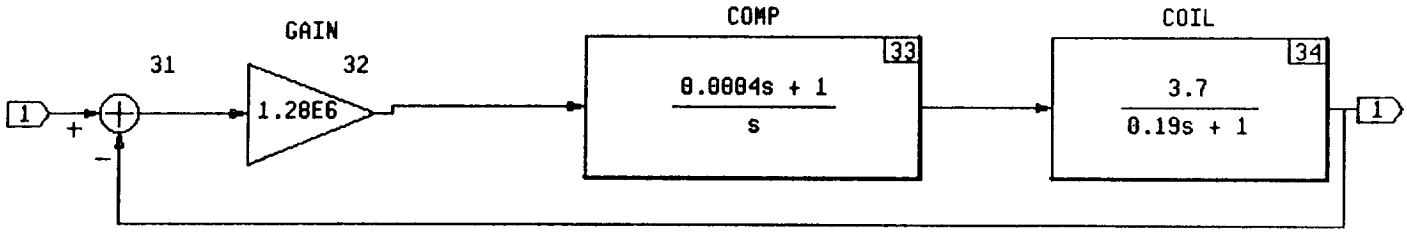

Figure 3-11. Computer Model of Actuator

Single Channel Analysis

The Z and Y channels are shown in Figures 3-12 and 3-13. Initial analysis was conducted on a single channel (Z channel without gyro coupling). An open loop analysis of the plant showed dominant dynamic characteristics as:

Poles	- 40, + 40, (- 200 ± i 4000)
Zeros	± i 900

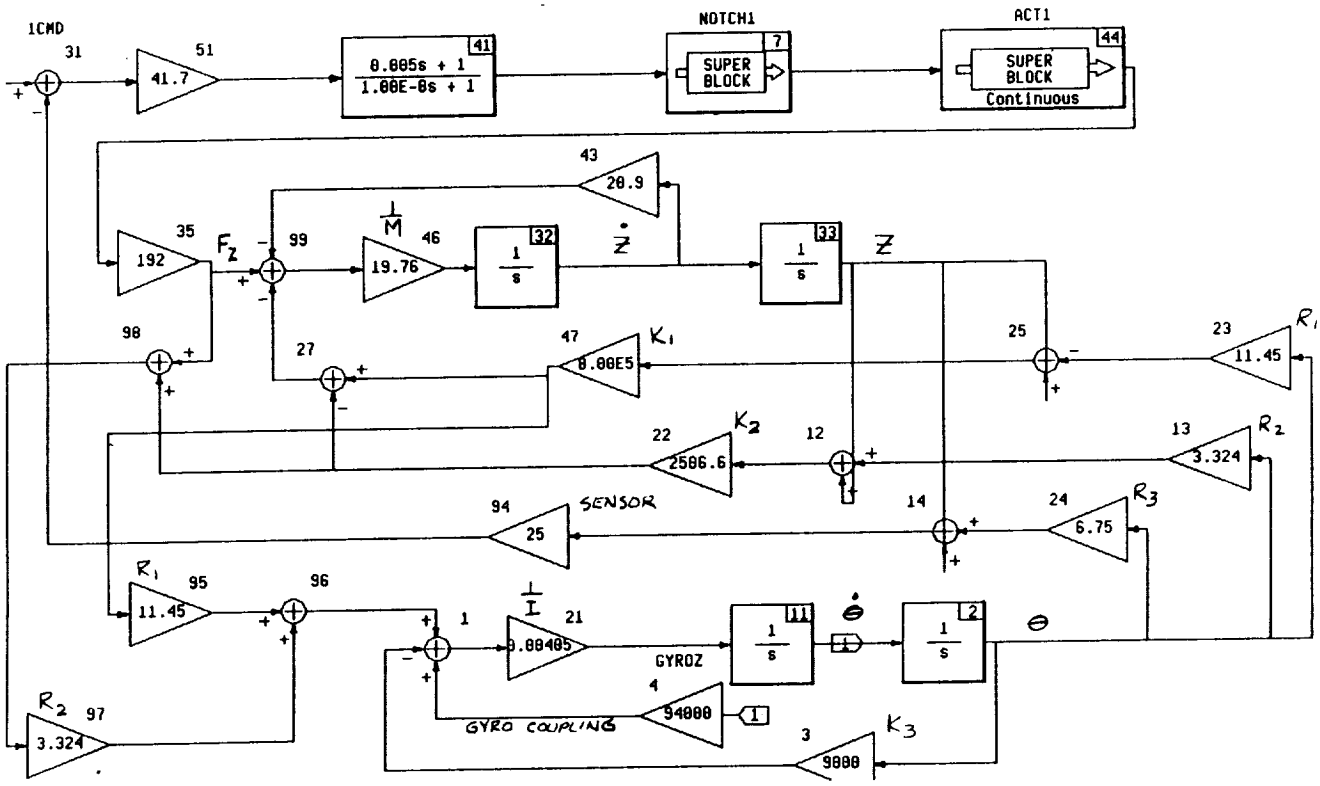

Figure 3-12. Z Channel Analysis

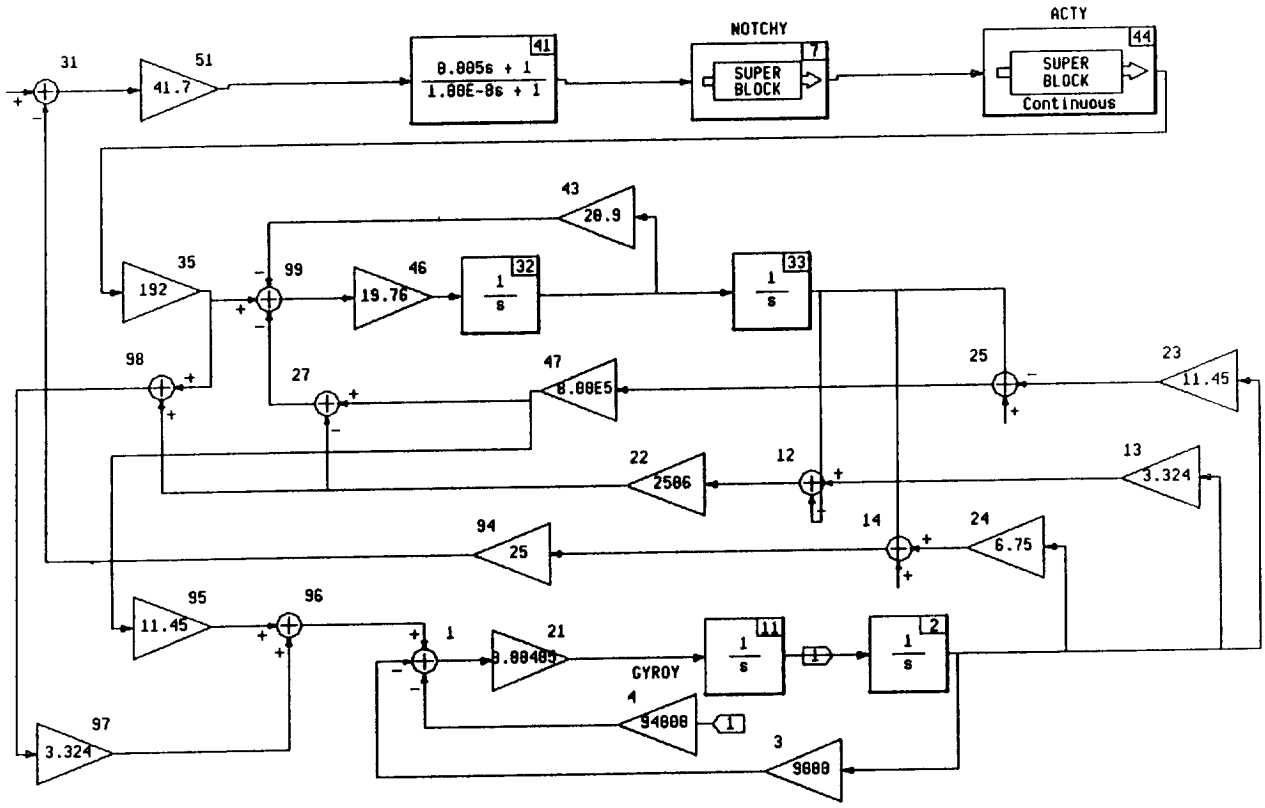

Figure 3-13. Y Channel Analysis

Without compensation, the poles at -40 would migrate to the zeros on the imaginary axis which would result in an oscillatory system. To move the roots into the negative real plane, a compensation pole was added at -200. The resulting root locus is shown in Figure 3-14a without the notch filter or actuator. Figure 3-14b shows the same root locus with the notch filter and actuator. It may be seen that the filter provides additional dynamic response and damping.

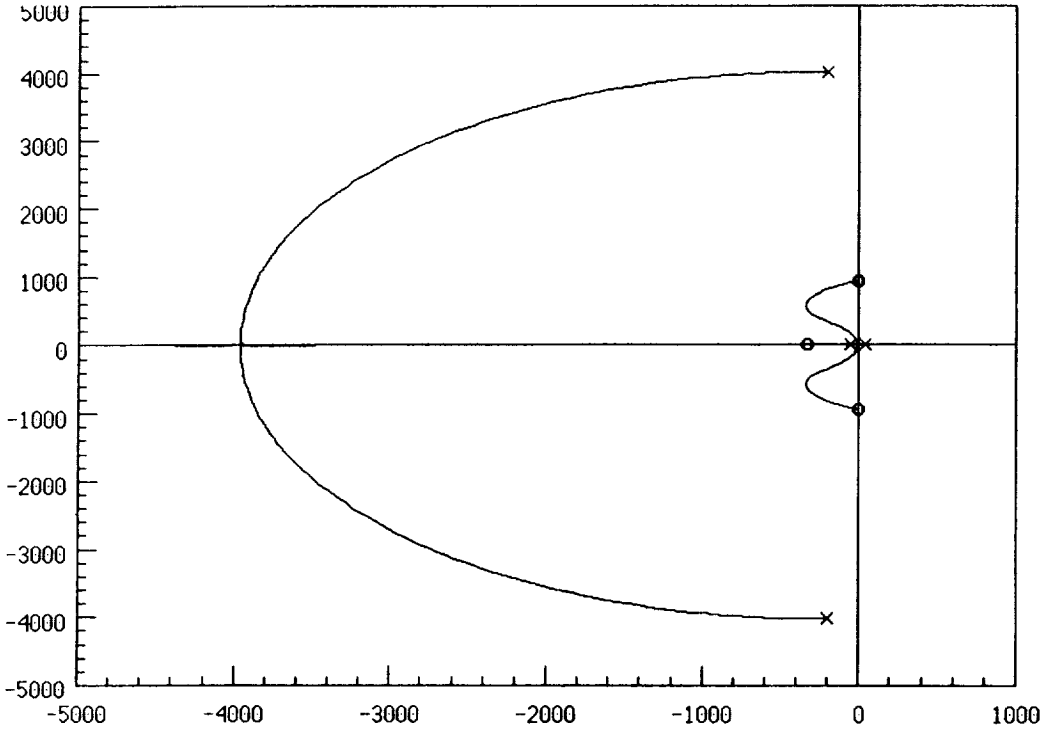

Figure 3-14a. Z Channel Root Locus, Without Notch Filter or Actuator

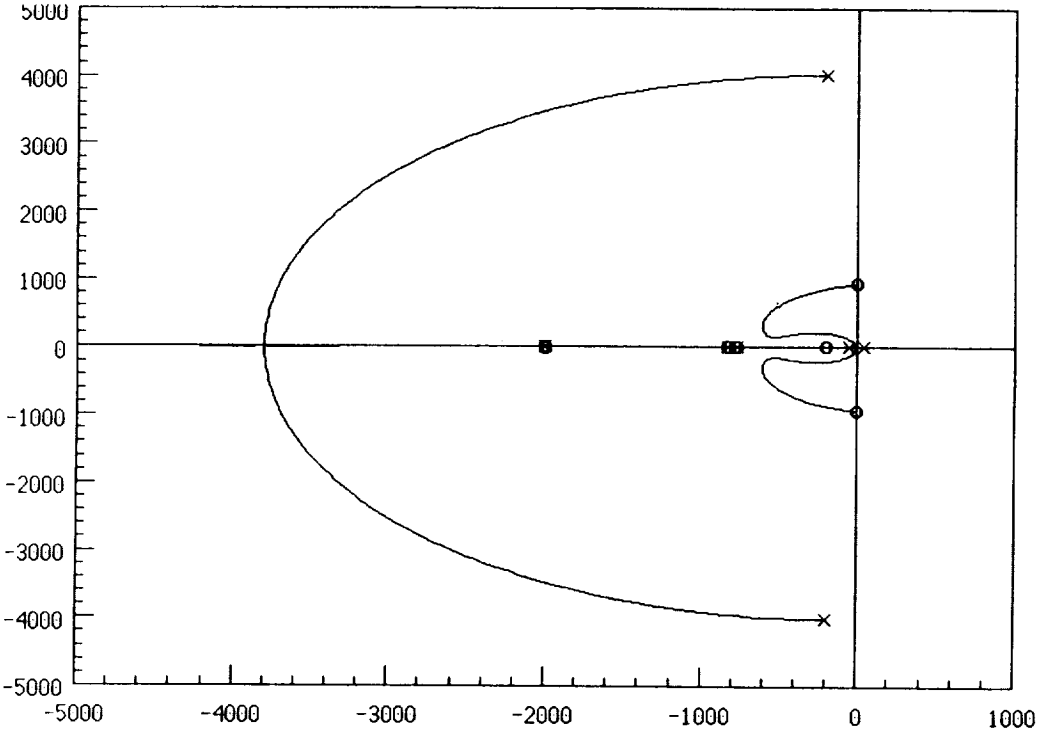

Figure 3-14b. Z Channel Root Locus, With Notch Filter and Actuator

Electronic gain was selected to provide the required stiffness of 200,000 lb/inch. With a sensor gain of 25 volts/inch, and a force constant of 192 lb/amp, the electronic gain is given as:

$$\text{Gain} = \frac{200000}{(192)(25)}$$

$$= 41.7$$

The resulting single channel closed loop Bode plot is shown in Figure 3-15. It may be seen that low frequency band width is at least 600 rad/sec, with adequate high frequency dynamic range for the actuator.

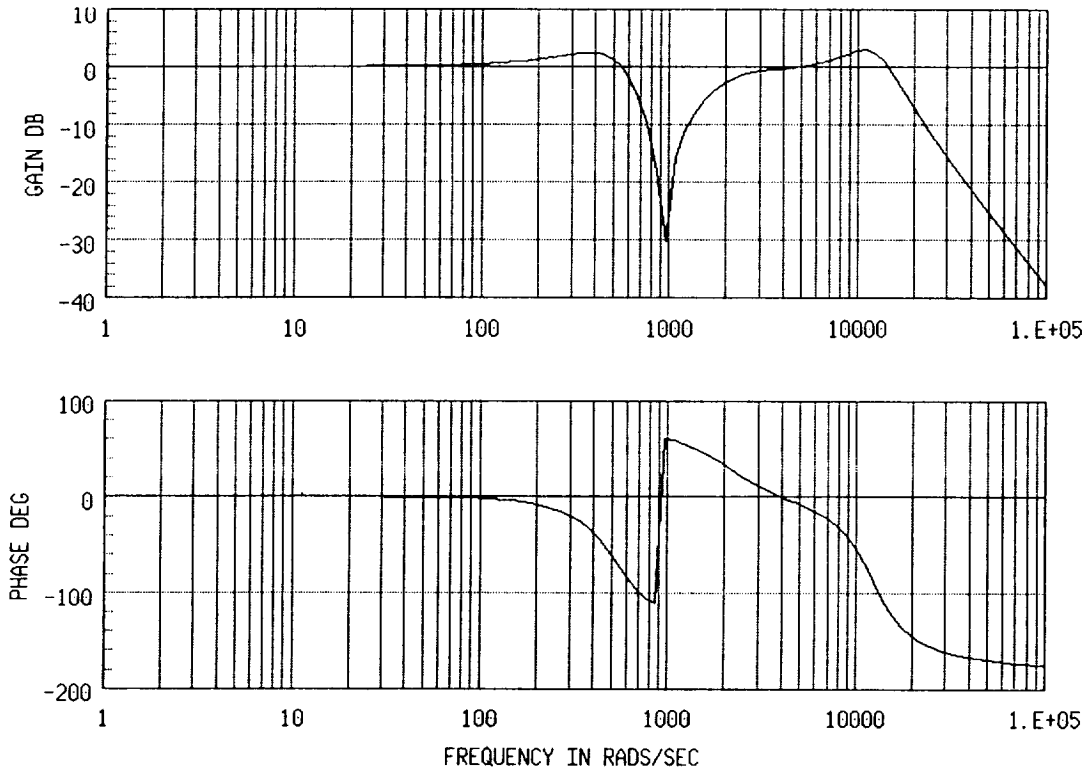

Figure 3-15. Single Channel Closed Loop Bode Plot

3.7 Lateral Force Generator

Input	Name	Output	Unit	Comment
18	awg			American wire gauge
2	tau			current density (.5 - 2mA/circ mil)
0.7	ffill		factor1	cavity fill factor
	a	1602	mu sq in	cross area bare wire circ mils
	fins	0.921	factor2	enamel insulation factor
	I	3.204	amps	current in wire
	NI	1161		amp windings
coilcav		0.9	sq inch	gross cavity area
	R70	0.817	Ohm	coil resistance
	n	362		number of windings
	11	4.2	inch	length av coil winding
	RT	0.82	Ohm	resistance at degrees F
70	deg F			coil temp
50	Fpole		lbs	Force per pole (2 poles/assy)
1.2	fringe		factor	fringing at pole
16	kGauss			magnetic ind at polegap
0.018	1gap		inch	gapwidth
250	Hz			forced frequency
	kMax	51	kMx	total magnetic flux
	reluct	22.98	Aw/kMx	coil reluctance (2 gaps)
	Apole	0.489	sq inch	pole area required
	L	0.057	Henry	Coil induction
	time	70	msec	time constant (L/R)
	Watts	8.379		Watts each coil
	Volts	2.62	Volts	Applied Voltage
	omega	1570.7963		$= 2\pi$ Hz
	C	7.0928E-6	Farad	Capacitor parallel with coil
1.2	d		inch	yoke height
1.7	hnet		inch	net assy height available
	w	0.408	inch	pole width
	b	1.39	inch	coil width
	h	0.646	inch	coil height
	OAwidth	2.21	inch	assy width

4.0 MAGNETIC BEARING RADIAL ACTUATOR ANALYSIS AND DESIGN

The design requires use of 28 MGO samarium cobalt magnet. The cylindrical pole pieces and shaft utilize low carbon cold rolled steel. The stator and rotor laminations will be punched from 0.014 thick vanadium permendure, heat treated for optimum magnetic performance.

The flux produced by the permanent magnet is forced through the four poles (each consisting of 3 teeth) and across a radial air gap into the rotor assembly. This flux then flows axially through the shaft and through another rotor and stator assembly identical to the first. The flux then returns through the opposite side of the magnet assembly.

The stator assembly has two pairs of poles that are 90 degrees to one another. Each pole is concentrically wound and connected so that a North and South pole are energized in series 180 degrees apart. With the control coils de-energized and the rotor magnetically centered, the net force on the rotor is zero. When a pair of poles in the X axis is energized, the flux under one pole adds to the permanent magnet flux and subtracts from the permanent magnet flux in the other pole. This action provides a force in the X axis proportional to the control current. Reversing the polarity of the control current reverses the X axis force. Similarly, the Y axis coils control Y axis forces.

The unit has been designed to produce a maximum force of 500 pounds (250 lbs on each end). The following tabulation lists the calculated performance characteristics:

Peak Force	500 lbs
Force Constant	385 lbs/Amp
Current @ 500 lbs	1.3 Amps
Resistance @ 20° C	14.0 Ω
Inductance (estimated)	75 mh
Negative Spring Constant	2510 lbs/in

Design Summary:

Magnet Assembly (O.D.)	5.25"
Magnet Assembly (I.D.)	3.50"
Magnet Thickness	0.35"
Stator (O.D.)	4.695/4.694"
Stator (I.D.)	3.030/3.029"
Stack Length	1.2"
Rotor (O.D.)	2.993/2.992"
Rotor (I.D.)	2.394/2.393"
Rotor Stack Length	1.3"

Mean air gap dia $= \frac{3.030 + 2.992}{2}$

$= 3.011$

Pole arc $= \frac{(3.011)(0.75)\,\pi}{4}$

$= 1.77$

Pole area $= (1.77)(1.2)$

$= 2.13\ \text{in.}^2$

$= 8.51\ \text{in.}^2$ (for 4 poles)

Magnet area (Am) $= \frac{((5.252)^2 - (3.52)^2)\,\pi}{4}$

$= 12.03$

$L_m = 0.350$

$A_g = 8.510$

$L_g = 0.036$ (2 gaps in series)

$B_g = \frac{B_r}{r_f \frac{L_g}{L_m} + \sigma \frac{A_g}{A_m}}$

Assume $r_f = 1.15$ (reluctance factor)

$\sigma = 1.80$ (leakage factor)

$B_g = \frac{10.5}{1.15 \frac{0.036}{0.35} + 1.8 \frac{8.51}{12.03}}$

$= 7.55$ Kgauss (48.7 Klines/in^2

$\frac{\phi}{\text{pole}} = (48.7)(8.51)$

$= 414$ Klines (Total of 4 poles)

Back iron x sect $= \dfrac{((5.2526)^2 - (4.695)^2)\,\pi}{4}$

$= 4.35\ in^2$

Back iron $B_{fe} = \dfrac{414}{4.35}$

$= 95.2\ Klines/in^2$

P/M Force/Pole $= \dfrac{(2.13)(48.72)^2}{72}$

$= 70.2\ lbs$

When magnetically centered, net force = 0

$F = \left(\dfrac{A}{72}\right)[(B_m + B_e)^2 - (B_m + B_e)]^2$

$= \dfrac{A}{18} B_m B_e$

$A = 2.13\ in^2$

$B_m = 48.7\ Klines/in^2$ (electro flux density)

$B_e =$ elecro flux density

$F = 250$ pounds

$= 5.76\ B_e$

$B_e = \dfrac{250}{5.76}$

$= 43.4\ Klines/in^2$

Assume $\sigma = 1.5$ in electromagnetic. circuit; ampere turns required in stator (2 poles in series):

$$N.I. = \frac{\sigma B_g}{0.00319}$$

$$= \frac{(1.5)(B_e)(0.036)}{0.00319}$$

$$= 16.9\ B_e$$

$$B_e = 0.059\ N.I.$$

$$F = 5.76\ B_e$$

$$= 0.034\ N.I.$$

$$K_f = F/I$$

$$= 0.34 \text{ Turns for 500 lbs} \qquad (250/\text{side})$$

$$\text{Required } K_f = \frac{250}{1.3}$$

$$= 192 \text{ lbs/amp}$$

$$\text{Turns} = \frac{192}{0.34}$$

$$= 564 \qquad \text{or 141 turns/coil (4 coils/axis)}$$

$$\phi/\text{pole} = 92.1 \times 2.13$$

$$= 196 \text{ Klines}$$

Vanadium Permendure laminations:

$$\text{Tooth thickness} = 0.416$$

$$B_{fe} = \frac{196}{(3)(1.2)(0.416)}$$

$$= 131 \text{ Klines/in}^2$$

Mean length of turn:

small coil = (0.75 + 1.2 + 0.4)(2)

= 4.7 inches

large coil = (2.00 + 1.2 + 0.4)(2)

= 7.2 inches

For 24 AWG copper wire, and 141 turns per coil:

R = (ohm/inch)(length of turn)(turns)

= (0.002139)(4.7 + 7.2)(2)(141)

= 7.18 ohms per pair of poles (@ 20° C)

= 14.36 ohms for coils in series

I = 1.3 amps for coils in series

Shaft flux density (assume same flux as in outer shell):

D = 2.393

$A = \frac{\pi (2.393)^2}{4}$

= 4.5 in^2

$B_{Fe} = \frac{416}{4.5}$

= 92.4 Klines/$in.^2$

Stator back iron and rotor:

Electromagnetic flux = (43.3) (2.13)
(@ 250 lbs) = 92.2 Klines

Flux splits two ways, or 46.1 Klines/path

Back iron thickness = $\frac{4.694 - 4.110}{2}$

$= 0.292$

Area $= (0.292)\ (1.2)$

$= 0.350$

B_{Fe} (back iron) $= \dfrac{46.1}{0.350}$

$= 132$ Klines/in.^{2}

B_{Fe} (rotor) $= \dfrac{46.1}{\dfrac{(2.992 - 2.393)\ (1.2)}{2}}$

$= 128$ Klines/in.^{2}

Negative Spring Constant:

Total magnetic force on each side of the target is due to the permanent magnets, or 70.5 lbs. The operating point of the magnet is at a permeance coefficient of:

$$Pc_0 = \frac{B_d}{H_d}$$

$$= \frac{(\sigma)\ (L_m)\ (A_g)}{(r_f)\ (L_g)\ (A_m)}$$

$$= \frac{(1.8)\ (0.350)\ (8.53)}{(1.15)\ (0.036)\ (12.03)}$$

$$= 10.8$$

With rotor displaced 0.015, (2 gaps = 0.030)

$$P_{c1} = (10.8)\left[\frac{0.036}{0.006}\right]$$

$$= 64.8$$

$$P_{c2} = (10.8)\left[\frac{0.036}{0.066}\right]$$

$$= 5.89$$

$$\Delta B_1 = 0.7 \text{ Kgauss}$$

$$\Delta B_2 = 0.6 \text{ Kgauss}$$

Magnet B = 9.8 Kgauss, so:

$$\text{Force (1)} = (70.2)\left[\frac{9.8 + 0.7}{9.8}\right]^2$$

$$= 80.6 \text{ lbs}$$

$$\text{Force (2)} = (70.2)\left[\frac{9.8 - 0.6}{9.8}\right]^2$$

$$= 61.8 \text{ lbs}$$

Net force @ 0.015 displacement:

$$= 80.6 - 61.8$$

$$= 18.8 \text{ lbs/side}$$

$$= 37.6 \text{ lbs total}$$

Negative Spring Constant:

$$= \frac{37.6}{0.015}$$

$$= 2507 \text{ lb/in.}$$

5.0 DESIGN, FABRICATION, AND ASSEMBLY OF CMBTF

A prototype model of the permanent magnet bias, actively controlled radial bearing concept was built to evaluate the feasibility and performance capability of the design. The prototype model used high efficiency cobalt-vanadium-iron alloy core material to provide the permanent magnet flux. The radial bearing consists of two field magnet stator assemblies made of 50% cobalt, 2% vanadium steel laminations. These field magnet assemblies were constructed using an existing motor lamination die, modified by removing four spokes (between each pole quadrant).

Hollow, circular cylindrical pole pieces of low carbon steel, magnetically connect the stator magnets to a hollow, circular cylinder, axially polarized, samarium cobalt permanent magnet. The shaft is made of martensitic, corrosion resistant steel and has two flywheels. The larger flywheel is used to achieve the desired rotor mass properties. The second flywheel, which is located at the shaft first critical speed antinode, is used to optimize the critical speed characteristics of the rotor.

Eddy current inductive position sensors are used to detect shaft position in the radial X and Y axes. A synchronous induction motor spins the rotor via a 2:1 belt drive. The bearing and servo control system is designed to operate at speeds up to 15,000 RPM.

A duplex pair ball bearing set is utilized at the lower end of the shaft to capture the rotor when the system is non-operational, or in the event of inadvertent power loss. The upper end of the rotor shaft is supported axially and radially by a DF duplex pair of ball bearings.

The test model has four horse-shoe shaped electromagnetic force generators in each quadrant to apply radial force to the bearing through the large flywheel. The force generators can apply loads up to 444.8 N (100 pounds) while the shaft is rotating.

The servo control electronics employs lead/lag compensation, and has a band width of approximately 250 Hz through the control coil inductive load. Conventional analog components were used in the breadboard prototype electronics. The servo control, including output power transistors and heat sinks, is contained in a package 4 x 4.5 x 6 inches and weighed 32 ounces.

6.0 CMBTF FUNCTIONAL TEST RESULTS

The feasibility test model was tested for performance characteristics at ambient conditions and speeds up to 2500 RPM. The results are summarized in Table 6-1.

Characteristic	Test Result
Load Capacity	2224 N (500 lb) at ambient temperature, linear to 1423 N (320 lb).
Radial Stiffness	Up to 0.79 x 10^4 N/mm (0.45 x 10^4 lb/in.)
Power Consumption	1.6 Watts into actuator, 17 Watts total (including servo electronics) at zero load and speeds up to 2500 RPM. 26 Watts into actuator at 1820 N load
Speed	2500 RPM at ambient (tests up to 15,000 RPM are planned at NASA Lewis Research Center)
Temperature Rise of Coils	No detectable temperature rise at currents up to 6.0 amps

Table 6-1. Results of Performance Tests

The load capacity at ambient conditions was tested up to a maximum of 1820 N (409 lbs). Load capacity testing was conducted by applying a load, through a strain gauge transducer, to the lower end of the shaft. Electronics input power and actuator current were measured with a wide band AC/DC digital power analyzer. Higher load testing was not done because of test fixture load capacity limitations. The magnetic bearing force output versus input control current is plotted in Figure 6-1, along with analytical predictions.

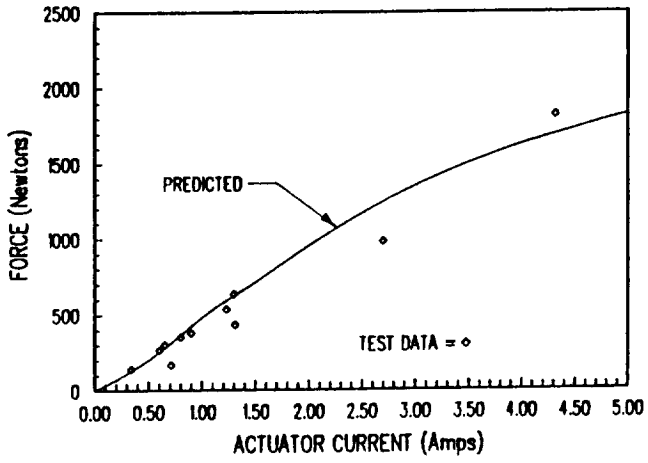

Figure 6-1. Load Output Vs. Input Current

The servo control electronics was designed to output a maximum of 5.0 amps, which from the analytical predictions shown in Figure 6-1 could produce an ambient temperature load capacity of 1820 N. The load capacity tests demonstrated 1820 N at a current of 4.3 amps. Therefore, testing at 5.0 amps is expected to show a load capacity greater than 2000 N.

Efforts were made to determine the temperature rise of the coils by measuring resistance change. With maximum currents of 5.0 amps applied up to 20 minutes, no change in resistance could be measured. This shows that the off-the-shelf motor lamination coil window could be further reduced with an optimum design lamination.

The power consumption of the new permanent magnet bias, actively controlled bearing actuator, was compared with that of the all-electromagnetic design (using cobalt, vanadium alloy), and the commercially available bearing of approximately equivalent load capacity. The AVCON design used from one to two orders of magnitude less power than either of the other bearings.

DESIGN CONCEPT	ZERO LOAD	MAX LOAD
New Permanent Magnet Bias Design	0.81 Watts	35.0 Watts
All-electromagnetic Actively Controlled Design (cobalt-vanadium)	90 Watts	380 Watts
Commercial, All-electromagnetic	95 Watts	400 Watts

Table 6-2. Magnetic Bearing Actuator Power Consumption at 70° F

7.0 SUMMARY AND CONCLUSIONS

The objectives of this program were to explore, via literature/industry survey analysis, and design/fabrication/test, the potential for using magnetic bearings in future SSME turbopumps.

The literature/industry survey showed that the optimal magnetic bearing was one based on permanent magnet bias, active magnet control. The survey further showed that the magnetic circuit should be homopolar and that the permanent magnet could be based on commercially available, high energy product materials, and that the system could operate in the linear portion of the magnetic materials B-H curve.

The analyses showed that the magnetic bearing could operate at ambient or cryogenic temperatures, that it could provide the required runouts, and that it could operate at low electrical consumption levels.

The design/fabrication was based on modifying an existing test rig. The modification involved converting the rig into a homopolar, permanent magnet bias, active control configuration. The lower conventional bearing was replaced by a radial magnetic bearing (permanent bias and active control). The design incorporated position sensors to sample the shaft displacements for the servo system stabilizing commands. Also, a conventional bearing was retained as a touchdown bearing for use prior to and after magnetic levitation, or in the event of power failure. The touchdown bearing was specifically designed to tolerate worst case mechanical and thermal conditions.

The rig upper bearing was retained, as well as the drive motor and drive belt mechanism.

The new design also incorporated magnetic lateral force generators so that the magnetic bearing could be tested against a variety of forces and force spectra which characterize the SSME environment.

Tests conducted on the rig at the contractor's facility included measurements of power dissipation under various load conditions, magnetic spring constant, radial runout, as well as determination of critical frequencies and demonstration of the ability of the servo system to cope with lateral loads.

The AVCON Homopolar Permanent Magent Bias design was found to be sufficiently small in size, weight, and power consumption to be considered for further development, although further weight reduction is required. The HPMB bearing was much more compact, was only one-third the weight, and had a power requirement much lower than competing designs.

Further technology advances (which are near term) will improve the characteristics of the magnetic bearing. For example, advances in permanent magnet materials will yield higher energy product permanent magnets to give larger biases, or provide the same bias with a smaller magnet.

Similarly, advances in digital servo control systems will permit operating the magnetic bearing nonlinearly, higher up on the B-H curve near saturation, so that more of the energy product can be used effectively. This, too, will give higher performance, and/or smaller magnetic bearings.

Also, digital servo systems can "memorize" systematic errors in the position sensor measurements (which may be due to target surface irregularities) and thus correct for these by means of table look-up schemes. This will lead to improved runout performance or relaxed specifications on the target surface finish characteristics.

After the CMBTF is demonstrated at cryogenic temperatures, we recommend that engineering development be undertaken to more correctly adapt magnetic bearings to SSME configurations and environments (dynamic as well as thermal and radiative).

We also recommend collateral exploration of the homopolar magnetic bearing approach to other NASA and commercial applications.

8.0 REFERENCES

1. Larson, Raymond K., "High Speed Machining: Taking Cutting Speeds One Step Beyond Iron Age", April 15, 1981.

2. Haberman H., and G. Laird, "An Active Magnetic Bearing System", SKF Industries Report, 1100 First Avenue, King of Prussia, PA, June 1981.

3. SKF Industries, Inc., "An Introduction to Active Magnetic Bearing Enables Optimum Damping of Flexible Rotor", ASME 29the International Gas Turbine Conference, Amsterdam, The Netherlands, June 4-7, 1984.

4. Haberman, H, and Maurice Brunet, "The Active Magnetic Bearing Enables Optimum Damping of Flexible Rotor", ASME 29the International Gas Turbine Conference, Amsterdam, The Netherlands, June 4-7, 1984.

5. Daniels, M. Gasser, A. Sherman, "Magnetically Suspended Stirling Cryogenic Space Refrigerator-Status Report", North American Philips Labs., Briarcliff, N.Y., NASA Goddard Space Flight Center, Greenbelt, MD.

6. Jayawant, V., "Electromagnetic Suspensions and Levitation", Edward Arnold, London, 1981.

7. Weh, Ing., "Linear Synchronous Motor Development for Urban and Rapid Transit Systems". IEEE Transactions on Magnetics, Vol. MAG-15, No. 6, November 1979.

8. Britcher, C.P. and M.J. Goodyer, "The Southampton University Magnetic Suspensions/Cryogenic Wind Tunnel Facility", Proceedings 1st International Symposium on Cryogenic Wind Tunnels, Southampton, England, April 3-5, 1979.

9. Wild, A., "Design Study and Development of a Magnetic Bearing Scanning Mechanism (MBSM) for Optical Sensor Applications", Final Report British Aerospace Aircraft Group, Hertforshire, England, May 1981.

10. Abbink, R.E., "Test of a Magnetic Bearing for Optical Scanner Applications", Report SLA-74-0347 Sandia Laboratories, Albuquerque, New Mexico, September 1974.

11. Sindlinger Rainer S., "Magnetic Bearing Momentum Wheels with Magnetic Gimballing Capability for 3-Axis Attitude Control and Energy Storage", paper presented at The 11th Aerospace Mech. Symp. NASA Goddard.

12. Earnshaw, S., "On The Nature of The Molecular Forces Which Regulate the Constitution of the Luminiferous Ether", Trans. Cambridge Phil Society, Vol. 7,97-112, 1842.

13. Backers, F.T., "A Magnetic Journal Bearing", Philips Technical Review, Volume 22, No. 7, 1961.

14. Meeks, C.R., "Magnetic Bearings - Optimum Design and Application", paper presented at International Workshop on Rare Earth Cobalt Permanent Magnets, University of Dayton, Dayton, Ohio, October 14-17, 1974.

15. Poubeau, P.C., "Satellite Flywheels with Magnetic Bearings and Passive Radial Centering", AIAA Journal of Spacecraft, Volume 17, No. 2, March-April 1980.

16. Auer, W., "Ball Bearing Versus Magnetic Bearings and Momentum Wheels as Momentum Actuators", paper presented at AIAA International Meeting & Technical Display Global Technology 2000, Baltimore, MD., May 6-8, 1980.

17. Poubeau, P.C., "Satellite Momentum and Reaction Wheels With Magnetic Bearings", Proceedings of AOCS Conference held in Noordwijk, October 3-6, 1977 (ESA SP-128, November 1977).

18. Poubeau, P.C. "Development of Satellite Flywheels Utilizing Magnetic Bearings With Passive Radial Centering - Concepts and Results", AIAA 78-571, Communications Satellite Systems Conference 7th, San Diego, CA, April 24-27, 1978.

19. Roters, "Electromagnetic Devices", John Wiley & Sons, New York, 1941.

20. Studer, P.A., "Magnetic Bearings for Instruments in the Space Environment", NASA Technical Memorandum 78048, NASA Goddard, 1978.

21. Studer, P.A., "A Practical Magnetic Bearing", IEEE Transactions on Magnetics, Vol. MAG-13, No. 5, Sept. 1977.

22. Murakami, C. et. al., "A New Type of Magnetic Gimballed Momentum Wheel and Its Application to Attitude Control in Space", Paper presented at 33rd Congress of Intl. Astronautical Federation, Paris, France, Sept. 27 - Oct. 2, 1982.

23. Knorrchen, H., and Th. Lange, "Modular Design and Dynamic Tests on Active Bearing Momentum Wheels", IFAC Automatic Controls in Space, Noordwiijkerhout, The Netherlands, 1982.

24. Albrecht, P., and Walowit, J.A., "A Theoretical and Experimental Investigation of the Magnetic Fields and Forces Arising in Magnetic Suspension Systems", Mechanical Technology, Inc. Report No. 75TR21, Jan., 1975.

REPORT DOCUMENTATION PAGE

Form Approved
OMB No. 0704-0188

1. AGENCY USE ONLY (*Leave blank*)	2. REPORT DATE	3. REPORT TYPE AND DATES COVERED
	February 1992	Final Contractor Report

4. TITLE AND SUBTITLE

Cryogenic Magnetic Bearing Test Facility (CMBTF)

5. FUNDING NUMBERS

WU–590–21–31
C–NAS3–25572

6. AUTHOR(S)

7. PERFORMING ORGANIZATION NAME(S) AND ADDRESS(ES)

AVCON – Advanced Controls Technology, Inc.
19151 Parthenia Street, Unit G
Northridge, California 91324

8. PERFORMING ORGANIZATION REPORT NUMBER

None

9. SPONSORING/MONITORING AGENCY NAMES(S) AND ADDRESS(ES)

National Aeronautics and Space Administration
Lewis Research Center
Cleveland, Ohio 44135–3191

10. SPONSORING/MONITORING AGENCY REPORT NUMBER

NASA CR–189087

11. SUPPLEMENTARY NOTES

Project Manager, Eliseo DiRusso, Structures Division, NASA Lewis Research Center, (216) 433–6027.

12a. DISTRIBUTION/AVAILABILITY STATEMENT

Unclassified - Unlimited
Subject Category 07

12b. DISTRIBUTION CODE

13. ABSTRACT (*Maximum 200 words*)

The Cryogenic Magnetic Bearing Test Facility (CMBTF) was designed and built to evaluate compact, lightweight magnetic bearings for possible use in space shuttle main engine liquid oxygen and liquid hydrogen turbopumps. State of the art and tradeoff studies were conducted which indicated that a hybrid permanent magnet bias homopolar magnetic bearing design would be smaller, lighter and much more efficient than conventional industrial bearings. A test bearing of this type was designed for the test rig for use at both room temperature and cryogenic temperature (–320 degrees F.). The bearing was fabricated from state-of-the-art materials and incorporated into the CMBTF. Testing at room temperature up to 2500 rpm was accomplished at Avcon's facility. These preliminary tests indicated that this magnetic bearing can be a feasible alternative to older bearing technologies. Analyses showed that the hybrid magnetic bearing is one-third the weight, considerably smaller and uses considerably less power than previous generations of magnetic bearings.

14. SUBJECT TERMS

Magnetic bearing; Active control; Vibration control; Damping; Rotor dynamics

15. NUMBER OF PAGES

66

16. PRICE CODE

A04

17. SECURITY CLASSIFICATION OF REPORT	18. SECURITY CLASSIFICATION OF THIS PAGE	19. SECURITY CLASSIFICATION OF ABSTRACT	20. LIMITATION OF ABSTRACT
Unclassified	Unclassified	Unclassified	